Fluctuating-surface-current formulation of radiative heat transfer: Theory and applications

Fluctuating-surface-current formulation of radiative heat transfer: Theory and applications

Alejandro W. Rodriguez,[1,2] M. T. H. Reid,[2] and Steven G. Johnson[2]
[1]*School of Engineering and Applied Sciences, Harvard University, Cambridge, Massachusetts 02138, USA*
[2]*Department of Mathematics, Massachusetts Institute of Technology, Cambridge, Massachusetts 02139, USA*
(Received 3 April 2013; published 30 August 2013)

We describe a fluctuating-surface current formulation of radiative heat transfer between bodies of arbitrary shape that exploits efficient and sophisticated techniques from the surface-integral-equation formulation of classical electromagnetic scattering. Unlike previous approaches to nonequilibrium fluctuations that involve scattering matrices—relating "incoming" and "outgoing" waves from each body—our approach is formulated in terms of "unknown" surface currents, laying at the surfaces of the bodies, that need not satisfy any wave equation. We show that our formulation can be applied as a spectral method to obtain fast-converging semianalytical formulas in high-symmetry geometries using specialized spectral bases that conform to the surfaces of the bodies (e.g., Fourier series for planar bodies or spherical harmonics for spherical bodies), and can also be employed as a numerical method by exploiting the generality of surface meshes/grids to obtain results in more complicated geometries (e.g., interleaved bodies as well as bodies with sharp corners). In particular, our formalism allows direct application of the boundary-element method, a robust and powerful numerical implementation of the surface-integral formulation of classical electromagnetism, which we use to obtain results in new geometries, such as the heat transfer between finite slabs, cylinders, and cones.

DOI: 10.1103/PhysRevB.88.054305 PACS number(s): 44.40.+a, 05.70.Ln, 12.20.−m

I. INTRODUCTION

Quantum and thermal fluctuations of charges in otherwise neutral bodies lead to stochastic electromagnetic (EM) fields everywhere in space. In systems at equilibrium, these fluctuations give rise to Casimir forces (generalizations of van der Waals interactions between macroscopic bodies), which have recently become the subject of intense theoretical and experimental work.[1–3] In nonequilibrium situations involving bodies at different temperatures, these fields also mediate energy exchange from the hotter to the colder bodies, a process known as *radiative heat transfer*. Although the basic theoretical formalism for studying heat transfer was laid out decades ago,[4–7] only recently have experiments reached the precision required to measure them at the microscale,[8–15] sparking renewed interest in the study of these interactions in complex geometries that deviate from the simple parallel-plate structures of the past.[16–23] In this manuscript, we present a novel formulation of radiative heat transfer for arbitrary geometries based on the well-known surface-integral-equation (SIE) formulation of classical electromagnetism,[24–27] which extends our recently developed fluctuating surface-current (FSC) approach to equilibrium Casimir forces[28] to the nonequilibrium problem of energy transfer between bodies of unequal temperatures. Unlike the scattering formulations based on basis expansions of the field unknowns best suited to special[29–35] or noninterleaved periodic[30,36–38] geometries, or formulations based on expensive, brute-force time-domain simulations[39] and Green's functions calculations,[40,41] this approach allows direct application of the boundary element method (BEM): a mature and sophisticated SIE formulation of the scattering problem in which the EM fields are determined by the solution of an algebraic equation involving a smaller set of surface unknowns (fictitious surface currents in the surfaces of the objects[24,26,27]).

A terse derivation of our FSC formulation for heat transfer was previously published in Ref. 42. The primary goals of this paper are to provide a more detailed presentation of this derivation and to generalize our previous formula for the heat transfer between two bodies to other situations of interest, including geometries consisting of multiple and/or nested bodies. We also demonstrate that the FSC framework can be applied as a spectral method to obtain semianalytical formulas in special geometries with high symmetry, as well as for purely numerical evaluation using BEM, which we exploit to obtain new results in a number of complicated geometries that prove challenging for semianalytical calculations. Although our formulation here employs similar guiding principles as our previous work on equilibrium Casimir phenomena[28,43]—both are based on the SIE framework of classical EM scattering—the heat-transfer case is by no means a straightforward extension of force calculations, because generalizing the equilibrium framework to nonequilibrium situations requires very different theoretical techniques. For example, the fact that in Ref. 28, we considered only *equilibrium* fluctuations made it possible for us to directly exploit the fluctuation-dissipation theorem for EM fields,[44] which relates the field-field correlation function at two points to a *single* Green's function between those two points. In contrast, although a fluctuation-dissipation theorem exists in the nonequilibrium problem, the field-field correlation functions are in this case determined by a product of two Green's functions integrated over the volumes of the bodies.[21,44] A key step in our derivation below is a correspondence between this volume integral (involving products of fields) and an equivalent surface integral involving the fictitious surface currents and fields of the SIE framework, that was not required in the equilibrium case.

The heat radiation and heat transfer of bodies with sizes and/or separations comparable to the thermal wavelength can deviate strongly from the predictions of the Stefan-Boltzmann law.[4,45] For instance, in the far field (object separations d much greater than the thermal wavelength $\lambda_T = \hbar c/k_B T$), radiative heat transfer is dominated by the exchange of propagating waves and is thus nearly insensitive to changes in separations (oscillations from interference effects typically

being small[5,46]). In the less-studied near-field regime ($d \lesssim \lambda_T$), not only are interference effects important, but otherwise-negligible evanescent waves also contribute flux through tunneling.[22,23] Such near-field effects have been most commonly studied in planar geometries, where the monotonically increasing contribution of evanescent waves with decreasing d results in orders-of-magnitude enhancement of the net radiative heat transfer rate (exceeding the far-field black-body limit at submicrometer separations[23]). This enhancement was predicted theoretically[5,22,23] and observed experimentally[47–49] decades ago in various planar structures, and has recently become the subject of increased attention due to its potential application in nanotechnology, with ramifications for thermal photovoltaics[50,51] and thermal rectification,[52–55] nanolithography,[56] thermally assisted magnetic recording,[57] and high-resolution surface imaging.[14,58,59] Thus far, there have been numerous works focused on the effects of material choice in planar bodies,[20,60] including studies of graphene sheets,[61] hyperbolic[62] and anisotropic materials,[36] and even materials exhibiting phase transitions,[63] to name a few. Along the same lines, many authors have explored transfer mediated by surface polaritons in thin films[64–67] and 1D-periodic planar bodies.[68] Despite decades of research, little is known about the near-field heat-transfer characteristics of bodies whose shapes differ significantly from these planar, unpatterned structures. Theoretical calculations were only recently extended to handle more complicated geometries, including spheres,[29,33] cylinders,[32] and cones[69] suspended above slabs, dipoles interacting with other dipoles[40,70–74] or with surfaces,[46,75–77] and also patterned/periodic surfaces.[30,31,39,42,78–80]

General-purpose methods for modeling heat transfer between bodies of arbitrary shapes can be distinguished in at least two ways, in the abstract *formulation* of the heat-transfer problem and in the *basis* used to "discretize" the formulation into a finite number of unknowns for solution on a computer (or by hand).[81] Theoretical work on heat transfer has mainly centered on "scattering-matrix' formulations, which express the heat transfer in terms of the matrices relating incoming and outgoing wave solutions from each body.[30–32,37,38,78] These formulations tend to be closely associated with "spectral' discretization techniques in which a Fourier-like basis (Fourier series, spectral harmonics, etc.) is used to expand the unknowns, because the incoming/outgoing waves must be expressed in terms of known solutions of Maxwell's equations, which are typically a spectral basis of plane waves, spherical waves, and so on. Such a spectral basis has the advantage that it can be extremely efficient (exponentially convergent) if the basis is specially designed for the geometry at hand (e.g., spherical waves for spherical bodies[29]). Scattering-matrix methods can also be used for arbitrary geometries, e.g., by expanding arbitrary periodic structures in Fourier series[30,37,78] or by coupling to a generic grid/mesh discretization to solve the scattering problems,[39,42,80] but exponential convergence no longer generally obtains. Furthermore, Fourier or spherical-harmonic bases of incoming/outgoing waves correspond to uniform angular/spatial resolution and require a separating plane/sphere between bodies, which can be a disadvantage for interleaved bodies or bodies with corners or other features favoring nonuniform resolution. In contrast to the geometric specificity encoded in a particular scattering basis, one extremely generic approach is a brute-force discretization of space and time, allowing one to solve for heat transfer by a Langevin approach[39] that handles all geometries equally, including geometries with continuously varying material properties. The FSC approach lies midway between these two extremes. Like the scattering-matrix approach, the FSC approach exploits the fact that one knows the EM solutions (Green's functions) analytically in homogeneous regions, so for piecewise-homogeneous geometries the only remaining task is to match boundary conditions at interfaces. Unlike the scattering-matrix approach, however, the FSC approach is formulated in terms of unknown surface currents rather than incoming/outgoing waves—the surface currents are arbitrary vector fields and need not satisfy any wave equation, which leads to great flexibility in the choice of basis. As described in this paper, the FSC formulation can use either a spectral basis or a generic grid/mesh and, as demonstrated in Refs. 42 and 80, works equally well for interleaved bodies (lacking a separating plane or even a well-defined notion of "incoming/outgoing' wave solutions). Moreover, the FSC formulation reduces the heat-transfer problem to a simple trace formula in terms of well-studied matrices that arise in SIE formulations of classical EM, which allows mature BEM solvers to be exploited with minimal additional computational effort.

The radiative heat transfer between two bodies 1 and 2 at local temperatures T^1 and T^2 can be written as[22,23]

$$H = \int_0^\infty d\omega\,[\Theta(\omega,T^1) - \Theta(\omega,T^2)]\Phi(\omega), \qquad (1)$$

where $\Theta(\omega,T) = \hbar\omega/[\exp(\hbar\omega/k_BT) - 1]$ is the Planck energy per oscillator at temperature T, and Φ is an ensemble-averaged *flux spectrum* into body 2 due to random currents in body 1 (defined more precisely below via the fluctuation-dissipation theorem[4,45,82]). (Physically, there are currents in both bodies, but EM reciprocity[83] means that one obtains the same Φ for flux into body 1 from sources in body 2; this also ensures that H obeys the second law of thermodynamics.) The only question is how to compute Φ, which naively involves a cumbersome number of scattering calculations.

The main result of this manuscript is the compact trace-formula for Φ derived in Sec. II, which involves standard matrices that arise in BEM calculations and forgoes any need for evaluation of fields or sources in the volumes of the bodies, separation of incoming and outgoing waves, integration of Poynting fluxes, or many scattering calculations. As explained below in Secs. III D and III C, by a slight modification of the two-body formula, one can also straightforwardly compute the spatially resolved pattern of Poynting flux on the surfaces of the bodies, as well as the emissivity of an isolated body. Section III A illustrates how important physical properties such as reciprocity and positivity of heat transfer manifest in the algebraic structure of the formulas. In Sec. III E, we generalize the two-body formula to also describe situations involving multiple and/or nested bodies. The remaining sections of the paper are devoted to validating the FSC formalism by checking it against known results in special geometries consisting of spheres and semi-infinite plates, as well as applying it to obtain new results in more complicated geometries consisting of finite slabs, cylinders, and cones. Specifically, Sec. IV B considers application of

the FSC formulation in high-symmetry geometries where the use of special-bases expansions involving Fourier and spherical-wave eigenfunctions (provided in Appendix A) leads to fast-converging semianalytical formulas of heat radiation and heat transfer for spheres and semi-infinite plates. In Secs. IV C and V, we exploit a sophisticated numerical implementation of the FSC formulation based on BEM to check the predictions of the semianalytical formulas in the case of spheres and to obtain new results in more complex geometries. Finally, the appendices at the end of the paper provide additional discussions that supplement and aid our derivations in Secs. II and III. Specifically, Appendix B provides a concise derivation of the principle of equivalence and its application to SIEs, and Appendices C 1 and C 2 provide succinct proofs of reciprocity and positivity of Green's functions and SIE matrices, respectively.

II. FSC FORMULATION

In this section, we review the SIE method of EM scattering and apply it to derive an FSC formulation of radiative heat transfer between two bodies. The result of this derivation is a compact trace expression for Φ involving SIE matrices. We further elaborate on these results in Sec. III, where we extend the formulation to handle other situations of interest, including the emissivity of isolated bodies, distribution of Poynting flux on the surfaces of the bodies, and heat transfer between multiple and/or nested bodies.

A. Notation

Let $\phi = \binom{\mathbf{E}}{\mathbf{H}}$ and $\sigma = \binom{\mathbf{J}}{\mathbf{K}}$ denote six-component volume electric and magnetic fields and currents, respectively, and ξ denote six-component *surface* currents (which technically have only four degrees of freedom since they are constrained to flow tangentially to the surfaces). In a homogeneous medium, fields are related to currents via convolutions ($\star$) with a 6×6 homogeneous Green's tensor $\Gamma(\mathbf{x},\mathbf{y}) = \Gamma(\mathbf{x}-\mathbf{y},\mathbf{0})$, such that $\phi = \Gamma \star (\sigma + \xi)$, or more explicitly

$$\phi(\mathbf{x}) = \int d^3\mathbf{y}\, \Gamma(\mathbf{x},\mathbf{y})[\sigma(\mathbf{y}) + \xi(\mathbf{y})], \tag{2}$$

where

$$\Gamma = \begin{pmatrix} \mathbf{\Gamma}^{EE} & \mathbf{\Gamma}^{EH} \\ \mathbf{\Gamma}^{HE} & \mathbf{\Gamma}^{HH} \end{pmatrix} = ik \begin{pmatrix} Z\,\mathbb{G} & \mathbb{C} \\ -\mathbb{C} & \frac{1}{Z}\mathbb{G} \end{pmatrix}$$

is the Green's tensor composed of 3×3 electric and magnetic Dyadic Green's functions (DGFs), determined by the "photon' DGFs $\mathbb{G}$ and $\mathbb{C}$. In the specific case of isotropic media (scalar ε and μ), $\mathbb{G}$ and $\mathbb{C}$ satisfy

$$[\nabla\times\nabla\times - k^2]\mathbb{G}(k;\mathbf{x},\mathbf{x}') = \delta(\mathbf{x}-\mathbf{x}')\mathbb{I}, \tag{3}$$

and $\mathbb{C} = \frac{i}{k}\nabla\times\mathbb{G}$, with wave number $k = \omega\sqrt{\varepsilon\mu}$ and impedance $Z = \sqrt{\mu/\varepsilon}$. Our derivation below applies to arbitrary linear anisotropic permittivity ε and permeability μ, so long as they are complex-symmetric matrices in order to satisfy reciprocity[84] (see Appendix C 1). The mathematical consequence of reciprocity, as described in the Appendix, is that Γ is complex-symmetric up to sign flips. In particular, $\Gamma(\mathbf{x},\mathbf{x}')^{\mathrm{T}} = \mathcal{S}\Gamma(\mathbf{x},\mathbf{x}')\mathcal{S}$, where the 6×6 matrix $\mathcal{S} = \mathcal{S}^{-1}$ flips the sign of the magnetic components. This reciprocity property is a key element of our derivation below.

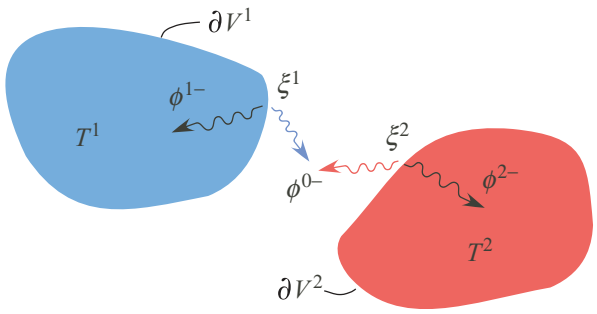

FIG. 1. (Color online) Schematic depicting two disconnected bodies described by surfaces ∂V^1 and ∂V^2 and held at temperature T^1 and T^2, respectively. Surface currents ξ^1 and ξ^2 laying on the surfaces of the bodies give rise to scattered fields ϕ^{1-} and ϕ^{2-}, respectively, in the interior of the bodies, and scattered field ϕ^{0-} in the intervening medium 0.

B. Surface integral equations

Consider the system depicted in Fig. 1, consisting of two homogeneous bodies, 1 and 2 (volumes V^1 and V^2 and temperatures T^1 and T^2), separated by a lossless medium 0 (volume V^0) by two interfaces ∂V^1 and ∂V^2, respectively. Consider also sources σ^r located in the interior of V^r and denote the total fields in each region by ϕ^r. The *homogeneous*-medium Green's functions for the infinite media in region r are denoted by Γ^r. Consider also the decomposition of the total fields ϕ^r in each region r into "incident' fields ϕ^{r+} (due to sources within r) and "scattered' fields ϕ^{r-} (from interactions with the other regions, including both scattering off the interface and sources in the other regions). That is, we can write $\phi^r = \phi^{r+} + \phi^{r-}$, with $\phi^{r+} = \Gamma^r \star \sigma^r$.

The core idea in the SIE formulation is the *principle of equivalence*,[24,85–89] whose derivation is briefly reprized in Appendix B, which states that the scattered field ϕ^{r-} can be expressed as the field of some *fictitious* electric and magnetic surface currents ξ^r located on the boundary of region r, acting within an infinite *homogeneous* medium r. In particular, one can write

$$\phi^0 = \phi^{0+} + \Gamma^0 \star (\xi^1 + \xi^2), \tag{4}$$

$$\phi^r = \phi^{r+} - \Gamma^r \star \xi^r, \tag{5}$$

for $r = 1,2$, with fictitious currents ξ^r completely determined by the boundary condition of continuous tangential fields at the body interfaces. Specifically, equating the tangential components of the total fields at the surfaces of the bodies, we find the *integral equations*:

$$(\Gamma^0 + \Gamma^r) \star \xi^r + \Gamma^0 \star \xi^{3-r}|_{\partial V^r} = \phi^{r+} - \phi^{0+}|_{\partial V^r}, \tag{6}$$

which can be solved to obtain ξ^r from the incident fields. This is the "PMCHW" surface-integral formulation of EM scattering.[24,90,91]

Let $\{\beta_n^r\}$ be a *basis* of six-component tangential vector fields on the surface of body r, so that any surface current ξ^r can be written in the form $\xi^r(\mathbf{x}) = \sum_n x_n^r \beta_n^r(\mathbf{x})$ for N coefficients $\{x_n^r\}$. (In BEM, β_n is typically a piecewise-polynomial

"element" function defined within discretized patches of each surface, most commonly the "RWG" basis functions.[92,93] However, one could just as easily choose β_n to be a spherical harmonic or some other "spectral" Fourier-like basis, as shown in Sec. IV B. The key point is that β_n is an arbitrary basis of surface vector fields; unlike scattering-matrix formulations, it need *not* consist of "incoming" or "outgoing" waves nor satisfy any wave equation.) Taking the inner product of both sides of Eq. (6) with β_m^r (a Galerkin discretization[94]), one obtains a matrix "BEM" equation of the form:

$$W^{-1}x = s, \tag{7}$$

where $x = \binom{x^1}{x^2}$ represents the expansion of the surface currents, $\xi^r = \sum_n x_n^r \beta_n^r$, $s = \binom{s^1}{s^2}$ describes the effect of the incident fields $s_m^r = \langle \beta_m^r, \phi^{r+} - \phi^{0+} \rangle$, and

$$\underbrace{\begin{pmatrix} W^{11} & W^{12} \\ W^{21} & W^{22} \end{pmatrix}^{-1}}_{W^{-1}} = \underbrace{\begin{pmatrix} G^{0,11} & G^{0,12} \\ G^{0,21} & G^{0,22} \end{pmatrix}}_{\hat{G}^0} + \underbrace{\begin{pmatrix} G^1 & \\ & 0 \end{pmatrix}}_{\hat{G}^1} + \underbrace{\begin{pmatrix} 0 & \\ & G^2 \end{pmatrix}}_{\hat{G}^2} \tag{8}$$

describes interactions with matrix elements $G_{mn}^{r,ij} = \langle \beta_m^i, \Gamma^r \star \beta_n^j \rangle$ among the basis functions. $\hat{G}^0$ represents multibody interactions between basis functions on *both* bodies, via waves propagating through the intervening medium 0. G^r represent self-interactions via waves propagating within a body, given by

$$G_{mn}^r \equiv G_{mn}^{r,rr} = \left\langle \beta_m^r, \Gamma^r \star \beta_n^r \right\rangle. \tag{9}$$

Here, $\langle \cdot, \cdot \rangle$ denotes the standard inner product $\langle \varphi, \psi \rangle = \int \varphi^* \psi$, with the $*$ superscripts denoting the conjugate-transpose (adjoint) operation.

A key property of the Green's function is reciprocity, as summarized and derived in Appendix C 2, and this property is reflected in symmetries of the matrices $\hat{G}$ and W. For simplicity, let us begin by considering the case of real-valued basis functions β_n. Let S be the matrix such that Sx flips the signs of the magnetic components (assuming that we either have separate basis functions for electric and magnetic components, as in the RWG basis, or more generally that the basis functions come in β_n and $\mathcal{S}\beta_n$ pairs). Note that $S^{-1} = S = S^{\mathrm{T}} = S^*$. In this case, as reviewed in Appendix C 2, it follows that $W^{\mathrm{T}} = SWS$ and $\hat{G}^{\mathrm{T}} = S\hat{G}S$. Once we have derived our heat-transfer formula for such real-valued basis functions, it is straightforward to generalize to complex-valued bases as described in Sec. III B.

C. Flux spectrum

Our goal is to compute the flux spectrum Φ into V^2 (the absorbed power in body 2) due to dipole current sources σ^1 in V^1 (integrated over all possible positions and orientations). We begin by considering Φ_{σ^1}, or the flux into body 2 due to a *single* dipole source σ^1 within body 1, corresponding to $\phi^{1+} = \Gamma^1 \star \sigma^1$, with $\phi^{0+} = \phi^{2+} = 0$. In the SIE (7), this results in a source term s with $s_m^1 = \langle \beta_m^1, \Gamma^1 \star \sigma^1 \rangle$ and $s^2 = 0$. As derived in Appendix B, the Poynting flux can be computed using the fact that ξ is actually equal to the surface-tangential fields,[25] $\xi = \binom{\mathbf{n} \times \mathbf{H}}{-\mathbf{n} \times \mathbf{E}}$, where $\mathbf{n}$ is the outward unit-normal vector. It follows that the integrated flux $-\frac{1}{2}\mathrm{Re} \oiint_2 (\overline{\mathbf{E}} \times \mathbf{H}) \cdot \mathbf{n} = \frac{1}{4}\mathrm{Re}\langle \xi^2, \phi^0 \rangle$. (This can also be derived as the power exerted on the surface currents by the total field, with an additional $1/2$ factor from a subtlety of evaluating the fields exactly on the surface.[89]) Hence

$$\Phi_{\sigma^1} = \tfrac{1}{4}\mathrm{Re}\langle \xi^2, \phi^0 \rangle = \tfrac{1}{4}\mathrm{Re}\langle \xi^2, \phi^2 \rangle = \tfrac{1}{4}\mathrm{Re}\langle \xi^2, -\Gamma^2 \star \xi^2 \rangle,$$

where we used the continuity of ϕ^0 and ϕ^2 and the fact that $\phi^{2+} = 0$. Substituting $\xi^2 = \sum_n x_n^2 \beta_n^2$ and recalling the definition of G^2 in Eq. (8), we obtain

$$\begin{aligned} \Phi_{\sigma^1} &= -\tfrac{1}{4}\mathrm{Re}(x^{2*} G^2 x^2) = -\tfrac{1}{4}\mathrm{Re}(x^* \hat{G}^2 x) \\ &= -\tfrac{1}{4}[x^* (\mathrm{sym}\hat{G}^2) x] = -\tfrac{1}{4} s^* W^* (\mathrm{sym}\hat{G}^2) W s \\ &= -\tfrac{1}{4}\mathrm{Tr}[s s^* W^* (\mathrm{sym}\hat{G}^2) W], \end{aligned}$$

where $\mathrm{sym}\, G = \frac{1}{2}(G + G^*)$ denotes the Hermitian part of G.

Computing Φ_{σ^1} is therefore straightforward for a single source σ^1. However, the total spectrum

$$\Phi = \langle \Phi_1 \rangle = -\tfrac{1}{4}\mathrm{Tr}[\langle s s^* \rangle W^* (\mathrm{sym}\hat{G}^2) W] \tag{10}$$

involves an ensemble-average $\langle \cdots \rangle$ over all sources σ^1 and polarizations in V^1. While this integration can be performed explicitly, we instead seek to simplify matters so that the final expression for Φ involves only surface integrals. The key point is that ss^* is an $N \times N$ matrix describing interactions among the N surface-current basis functions. The ensemble average $\langle ss^* \rangle$ is also an $N \times N$ matrix, which we would like to express in terms of a simple scattering problem involving the SIE Green's function matrices, hence eliminating any explicit computations over the interior volume V^1.

Defining the Hermitian matrix $\hat{C} = \langle ss^* \rangle$, it follows that its only nonzero entries lie in the upper-left $N_1 \times N_1$ block $C^1 = \langle s^1 s^{1*} \rangle$ and are given by $C_{mn}^1 = \langle s_m^1 \overline{s_n^1} \rangle = \langle \langle \beta_m^1, \Gamma^1 \star \sigma^1 \rangle \langle \Gamma^1 \star \sigma^1, \beta_n^1 \rangle \rangle$, or

$$\begin{aligned} C_{mn}^1 &= \left\langle \oiint d^2\mathbf{x} \iiint d^3\mathbf{y} \beta_m^1(\mathbf{x})^{\mathrm{T}} \Gamma^1(\mathbf{x},\mathbf{y}) \sigma^1(\mathbf{y}) \oiint d^2\mathbf{x}' \iiint d^3\mathbf{y}' \sigma^1(\mathbf{y}')^* \Gamma^1(\mathbf{x}',\mathbf{y}')^* \beta_n^1(\mathbf{x}') \right\rangle \\ &= \oiint d^2\mathbf{x} \iiint d^3\mathbf{y} \beta_m^1(\mathbf{x})^{\mathrm{T}} \Gamma^1(\mathbf{x},\mathbf{y}) \oiint d^2\mathbf{x}' \iiint d^3\mathbf{y}' \langle \sigma^1(\mathbf{y}) \sigma^1(\mathbf{y}')^* \rangle \Gamma^1(\mathbf{x}',\mathbf{y}')^* \beta_n^1(\mathbf{x}') \\ &= \frac{4}{\pi} \oiint d^2\mathbf{x} \iiint d^3\mathbf{y} \oiint d^2\mathbf{x}' \beta_m^1(\mathbf{x})^{\mathrm{T}} \Gamma^1(\mathbf{x},\mathbf{y}) [\omega \mathrm{Im}\chi(\mathbf{y})] \Gamma^1(\mathbf{x}',\mathbf{y})^* \beta_n^1(\mathbf{x}'), \end{aligned} \tag{11}$$

where in the third line we have performed an integration over all dipole positions by employing the fluctuation-dissipation theorem[82] for the current-current correlation function,

$$\langle \sigma^1(\mathbf{y})\sigma^1(\mathbf{y}')^* \rangle = \frac{4}{\pi}\omega \mathrm{Im}\chi(\mathbf{y},\omega)\delta(\mathbf{y}-\mathbf{y}'), \tag{12}$$

and where we omitted the dependence on the Planck energy distribution $\Theta(\omega,T)$, which has been factored out into Eq. (1), and where $\mathrm{Im}\chi$ denotes the imaginary part of the 6×6 material susceptibility tensor, so that $\mathrm{Im}\chi = \left(\begin{smallmatrix} \mathrm{Im}\varepsilon & 0 \\ 0 & \mathrm{Im}\mu \end{smallmatrix}\right)$, which is related to material absorption.

Equation (11) closely resembles an absorbed power in the volume of body 1, since absorbed power for a field ϕ is $\frac{1}{2}\int \phi^*(\omega \mathrm{Im}\chi)\phi$.[83] To make this analogy precise, some careful algebraic manipulation is required, and the abovementioned reciprocity relations [$\Gamma(\mathbf{x},\mathbf{x}')^{\mathrm{T}} = \mathcal{S}\Gamma(\mathbf{x},\mathbf{x}')\mathcal{S}$, $W^{\mathrm{T}} = SWS$, etc.] play a key role. In particular, the fact that C^1 is Hermitian implies that the matrix is completely determined by the values of $x^{1*}S(C^1)^{\mathrm{T}}Sx^1$ for all x^1, where we have inserted the sign-flip matrices S and the transposition for later convenience. Interpreting x^1 as the basis coefficients of a surface current $\xi^1 = \sum_n x_n^1 \beta_n^1$ on ∂V^1, we find

$$\begin{aligned}
x^{1*}S(C^1)^{\mathrm{T}}Sx^1 &= \langle |x^{1*}S\overline{s^1}|^2\rangle = \langle |\xi^1, S\overline{\Gamma^1 \star \sigma^1}|^2\rangle \\
&= \oiint d^2\mathbf{x} \iiint d^3\mathbf{y} \oiint d^2\mathbf{x}' \iiint d^3\mathbf{y}' \xi^1(\mathbf{x})^* S\overline{\Gamma^1(\mathbf{x},\mathbf{y})}\langle \overline{\sigma^1(\mathbf{y})}\sigma^1(\mathbf{y}')^{\mathrm{T}}\rangle \Gamma^1(\mathbf{x}',\mathbf{y})^{\mathrm{T}} S\xi^1(\mathbf{x}') \\
&= \frac{4}{\pi}\oiint d^2\mathbf{x} \iiint d^3\mathbf{y} \oiint d^2\mathbf{x}' \xi^1(\mathbf{x})^* \mathcal{S}\overline{\Gamma^1(\mathbf{x},\mathbf{y})}[\omega \mathrm{Im}\chi(\mathbf{y})]\mathcal{S}\Gamma^1(\mathbf{x}',\mathbf{y})\xi^1(\mathbf{x}') \\
&= \frac{4}{\pi}\oiint d^2\mathbf{x} \iiint d^3\mathbf{y} \oiint d^2\mathbf{x}' \xi^1(\mathbf{x})^* \mathcal{S}\overline{\Gamma^1(\mathbf{x},\mathbf{y})}\mathcal{S}[\omega \mathrm{Im}\chi(\mathbf{y})]\Gamma^1(\mathbf{x}',\mathbf{y})\xi^1(\mathbf{x}') \\
&= \frac{4}{\pi}\oiint d^2\mathbf{x} \iiint d^3\mathbf{y} \oiint d^2\mathbf{x}' [\Gamma^1(\mathbf{y},\mathbf{x})\xi^1(\mathbf{x})]^*[\omega \mathrm{Im}\chi(\mathbf{y})][\Gamma^1(\mathbf{x}',\mathbf{y})\xi^1(\mathbf{x}')] \\
&= \frac{4}{\pi}\langle \Gamma^1 \star \xi^1, (\omega \mathrm{Im}\chi)\Gamma^1 \star \xi^1\rangle,
\end{aligned} \tag{13}$$

where in the first and fourth lines, we invoked reciprocity (from above) and in the third line, we assumed that $\mathcal{S}$ commutes with $\mathrm{Im}\chi$, which is true for reciprocal media. (The only way that $\mathcal{S}$ would not commute with $\mathrm{Im}\chi$ would be if there were a chiral susceptibility coupling electric and magnetic fields directly, also called a bianisotropic susceptibility, which breaks reciprocity.[95]) Letting $\phi^1 = \Gamma^1 \star \xi^1$ be the field due to the surface current ξ^1, it follows that

$$x^{1*}S(C^1)^{\mathrm{T}}Sx^1 = \frac{4}{\pi}\langle \phi^1, (\omega \mathrm{Im}\chi)\phi^1\rangle. \tag{14}$$

But, as noted above, $\frac{1}{2}\langle \phi^1, \omega(\mathrm{Im}\chi)\phi^1\rangle$ (where the inner product $\langle\cdot,\cdot\rangle$ is now over the volume V^1) has a simple meaning: it is the *absorbed power* in V^1 from the currents ξ^1, or equivalently, the time-average power density dissipated in the interior of body 1 by the field ϕ^1 produced by ξ^1.

Computing the interior dissipated power from an *arbitrary* surface current turns out to be somewhat complicated, since one needs to take into account the possibility that the equivalent surface currents arise from sources both outside and inside V^1. If, on the other hand, we could restrict ourselves to equivalent currents ξ^1 that are outside of V^1, then we can use the result from above that the incoming Poynting flux (the absorbed power) is simply $-\frac{1}{4}\mathrm{Re}\langle \xi^1, \phi^1\rangle = -\frac{1}{4}x^{1*}(\mathrm{sym}G^1)x^1$. Substituting this into Eq. (14), we would be immediately led to the identity $x^{1*}S(C^1)^{\mathrm{T}}Sx^1 = -\frac{2}{\pi}\mathrm{Re}\,(x^{1*}G^1x^1)$, and this gives an expression for C^1 in terms of G^1. It turns out that indeed, we need not handle arbitrary ξ^1 since the $\hat{C}$ matrix is never used by itself—it is only used in the trace expression

$$\begin{aligned}
\Phi &= -\tfrac{1}{4}\mathrm{Tr}[\hat{C}W^*(\mathrm{sym}\hat{G}^2)W] = -\tfrac{1}{4}\mathrm{Tr}[\cdots]^{\mathrm{T}} \\
&= -\tfrac{1}{4}\mathrm{Tr}[SWSS(\mathrm{sym}\hat{G}^2)SSW^*S\hat{C}^{\mathrm{T}}] \\
&= -\tfrac{1}{4}\mathrm{Tr}[SW(\mathrm{sym}\hat{G}^2)W^*S\hat{C}^T] \\
&= -\tfrac{1}{4}\mathrm{Tr}[S\hat{C}^{\mathrm{T}}SW(\mathrm{sym}\hat{G}^2)W^*],
\end{aligned} \tag{15}$$

using reciprocity. As shown in Sec. III A, the standard definiteness properties of the Green's functions (currents do nonnegative work) imply that $\mathrm{sym}\hat{G}^r$ is negative semidefinite and hence admits a Cholesky factorization[96] $\mathrm{sym}\hat{G}^r = -\hat{U}^{r*}\hat{U}^r$. It follows that Eq. (15) can be written as $-\frac{1}{4}\mathrm{Tr}[X^*S\hat{C}^{\mathrm{T}}SX]$, where $X = W\hat{U}^{2*}$ are the "currents" due to "sources" represented by the columns of $\hat{U}^{2*}$, which are all of the form $\left(\begin{smallmatrix} 0 \\ s^2 \end{smallmatrix}\right)$: currents from sources in V^2 alone. So, effectively, $S\hat{C}^{\mathrm{T}}S$ is only used to evaluate the power dissipated in V^1 from sources in V^2, and by the same Poynting-theorem reasoning from above, it follows that $S(C^1)^{\mathrm{T}}S = -\frac{2}{\pi}\mathrm{sym}G^1$, and hence

$$\hat{C} = -\frac{2}{\pi}\mathrm{sym}S(\hat{G}^1)^{\mathrm{T}}S = -\frac{2}{\pi}\mathrm{sym}\hat{G}^1 \tag{16}$$

by the symmetry of $\hat{G}^1$. Substituting this result into Eq. (10) then gives the heat-transfer formulation summarized in the next section.

D. Heat-transfer formula

The result of the above derivation is that the ensemble-averaged flux from V^1 to V^2 can be expressed in the compact

form

$$\Phi = \frac{1}{2\pi}\mathrm{Tr}[(\mathrm{sym}\hat{G}^1)W^*(\mathrm{sym}\hat{G}^2)W] \quad (17)$$

$$= \frac{1}{2\pi}\mathrm{Tr}[(\mathrm{sym}G^1)W^{21*}(\mathrm{sym}G^2)W^{21}], \quad (18)$$

with W^{21} relating incident fields at the surface of body 2 to the equivalent currents at the surface of body 1. Our simplified expression is computationally convenient because it only involves standard matrices that arise in BEM calculations,[26] with no explicit need for evaluation of fields or sources in the volumes,[29,39,40] separation of incoming and outgoing waves,[30–32,37,38,78] integration of Poynting fluxes,[39] or any additional scattering calculations.

III. GENERALIZATIONS

In this section, we study the positivity and symmetries of the two-body heat-transfer formula above and consider generalizations to include other situations of interest. Following similar arguments as those employed in the previous section, we derive formulas for the emissivity of isolated bodies, the spatial distribution of Poynting flux on the surfaces of bodies, and the heat transfer between multiple and nested bodies. In Sec. III B, we show that abandoning our choice of real-β basis functions above in favor of complex-β functions does not change the final formula for Φ, so long as the βs come in complex conjugate pairs.

A. Positivity and reciprocity

In addition to its computational elegance, Eq. (18) algebraically captures crucial physical properties of the flux spectrum: Φ is *positive-definite* $\Phi \geqslant 0$ and symmetric with respect to $1 \leftrightarrow 2$ exchange, as required by *reciprocity*. Of course, the positivity of Φ is immediately clear from the Rytov starting point of fluctuating currents inside the bodies: the absorbed power in one body from sources in the other body is simply $\sim\int(\omega\mathrm{Im}\epsilon)|\mathbf{E}|^2 \geqslant 0$ (since $\omega\,\mathrm{Im}\epsilon \geqslant 0$ for passive media[83,84]). Hence positivity must hold for any formulation that is mathematically equivalent to the Rytov picture. However, it is still useful and nontrivial to understand how this positivity manifests itself algebraically in a given formulation. For example, Ref. 35 showed how positivity manifests itself in a scattering-matrix framework. In our FSC framework, positivity turns out to correspond to the fact that Φ can be interpreted as a kind of matrix norm.

As derived above, the standard definiteness properties of the Green's functions (currents do nonnegative work) imply that $\mathrm{sym}G^r$ is negative semidefinite and hence admits a Cholesky factorization $\mathrm{sym}G^r = -U^{r*}U^r$, where U^r is upper-triangular. It follows that

$$\Phi = \frac{1}{2\pi}\mathrm{Tr}[U^1W^*U^{2*}U^2WU^{1*}]$$

$$= \frac{1}{2\pi}\mathrm{Tr}[Z^*Z] = \frac{1}{2\pi}\|Z\|_F^2, \quad (19)$$

where $Z = U^2WU^{1*}$, is a weighted Frobenius norm of the SIE matrix W, which from above we know is necessarily non-negative.

Furthermore, reciprocity (symmetry of Φ under $1 \leftrightarrow 2$ interchange) corresponds to simple symmetries of the matrices. As derived in Appendix C 1, $\Gamma(\mathbf{y},\mathbf{x})^{\mathrm{T}} = \mathcal{S}\Gamma(\mathbf{x},\mathbf{y})\mathcal{S}$, $\hat{G}^{\mathrm{T}} = S\hat{G}S$, and $W^{\mathrm{T}} = SWS$, where $S = S^{\mathrm{T}} = S^{-1} = S^*$ is the matrix that flips the signs of the magnetic basis coefficients and swaps the coefficients of β_n and $\overline{\beta_n}$. It follows that

$$\Phi = \frac{1}{2\pi}\mathrm{Tr}[SWS(\mathrm{sym}S\hat{G}^2S)SW^*S(\mathrm{sym}S\hat{G}^1S)]$$

$$= \frac{1}{2\pi}\mathrm{Tr}[(\mathrm{sym}\hat{G}^2)W^*(\mathrm{sym}\hat{G}^1)W], \quad (20)$$

where the S factors cancel, leading to the $1 \leftrightarrow 2$ exchange.

B. Complex-valued basis functions

For convenience, we assumed above that the basis functions β_n were purely real-valued. However, it easy to generalize the final result *a posteriori* to complex-valued basis functions. The relevant case to consider are basis functions that come in complex-conjugate pairs β_n and $\beta_{n'} = \overline{\beta_n}$ (true for any practical complex basis). Such a basis can always be transformed into an equivalent real-valued basis $\tilde{\beta}_n$ by the linear transformation $\tilde{\beta}_n = \frac{1}{\sqrt{2}}(\beta_n + \beta_{n'})$ and $\tilde{\beta}_{n'} = \frac{i}{\sqrt{2}}(\beta_n - \beta_{n'})$. In an expansion $\xi = \sum_n x_n\beta_n = \sum_n \tilde{x}_n\tilde{\beta}_n$, this is simply a rotation $\tilde{x} = Qx$ where the matrix Q is easily verified to be unitary ($Q^* = Q^{-1}$), since it is composed of unitary 2×2 blocks (operating on n,n' complex-conjugate pairs). Given such a unitary change of basis, we can make a corresponding unitary change to the G and W matrices from above, $\tilde{G} = Q\hat{G}Q^*$ and $\tilde{W} = QWQ^*$, to obtain the matrices in the complex basis. By inspection of the Φ expression above, all of the Q factors cancel after the change of basis and one obtains the same expression in the complex basis with the new $\tilde{G}$ and $\tilde{W}$ matrices.

C. Emissivity of a single body

The same formalism can be applied to compute the emissivity of a single body. For a *single* body 1 in medium 0, the emissivity of the body is the flux Φ^0 of random sources in V^1 into V^0.[23] Following the derivation above, the flux into V^0 is $-\frac{1}{4}\mathrm{Re}\langle\xi^1,\phi^0\rangle = -\frac{1}{4}\langle\xi^1,\Gamma^0\star\xi^1\rangle$. The rest of the derivation is essentially unchanged except that $W = (G^1 + G^0)^{-1}$ since there is no second surface. Hence we obtain

$$\Phi^0 = \frac{1}{2\pi}\mathrm{Tr}[(\mathrm{sym}G^1)W^*(\mathrm{sym}G^0)W], \quad (21)$$

which again is invariant under $1 \leftrightarrow 0$ interchange from the reciprocity relations (Kirchhoff's law).

D. Surface Poynting-flux pattern

It is also interesting to consider the spatial distribution of Poynting-flux pattern, which can be obtained easily because, as explained above, $\frac{1}{4}\mathrm{Re}[\xi^2(\mathbf{x})^*\phi^2(\mathbf{x})]$ is exactly the inward Poynting flux at a point $\mathbf{x}$ on surface 2. It follows that the mean

contribution Φ_n^2 of a basis function β_n^r to Φ is

$$\begin{aligned}\Phi_n^2 &= -\frac{1}{4}\langle \mathrm{Re}\big[s^* W^* e_n^2 e_n^{2*} \hat{G}^2 W s\big]\rangle \\ &= -\frac{1}{4}\mathrm{Re}\big[e_n^{2*}\hat{G}^2 W \langle s s^*\rangle W^* e_n^2\big] \\ &= \frac{1}{2\pi}\mathrm{Re}\big[e_n^{2*}\hat{G}^2 W(\mathrm{sym}\hat{G}^1)W^* e_n^2\big],\end{aligned}$$

where e_n^2 is the unit vector corresponding to the β_n^2 component. This further simplifies to $\Phi_n^2 = F_{nn}^2$, where

$$F^2 = \frac{1}{2\pi}\mathrm{Re}[G^2 W^{21}(\mathrm{sym}G^1)W^{21*}]. \tag{22}$$

Note that $\Phi = \mathrm{Tr}F^2$. Similarly, by swapping $1 \leftrightarrow 2$, we obtain a matrix F^1 such that $\Phi_n^1 = F_{nn}^1$ is the contribution of β_n^1 to the flux on surface ∂V^1.

E. Multiple and nested bodies

In this section, we extend the FSC formalism above to situations involving multiple and nested bodies. For simplicity, we only consider an additional medium 3, since generalizations to include additional bodies or levels of nesting readily follow. Because the derivation is almost identical to the two-body case, we only focus on those aspects that differ.

1. Multiple bodies

Consider the system depicted in Fig. 2, consisting of three disconnected bodies at different temperatures. Applying the principle of equivalence, one finds

$$\phi^0 = \phi^{0+} + \Gamma^0 \star (\xi^1 + \xi^2 + \xi^3), \quad \phi^r = \phi^{r+} - \Gamma^r \star \xi^r,$$

for $r = 1,2,3$, with fictitious currents ξ^r determined by the boundary conditions of continuous tangential fields at the body interfaces. Equating the tangential components of the fields at the surfaces of the bodies, one obtains the integral equations:

$$(\Gamma^0 + \Gamma^r)\star\xi^r + \sum_{i\neq r}(\Gamma^0 \star \xi^j)|_{\partial V^r} = \phi^{r+} - \phi^{0+}|_{\partial V^r}, \tag{23}$$

along with the corresponding SIE matrix:

$$\begin{aligned}&\underbrace{\begin{pmatrix} W^{11} & W^{12} & W^{13} \\ W^{21} & W^{22} & W^{23} \\ W^{31} & W^{32} & W^{33}\end{pmatrix}^{-1}}_{W^{-1}} \\ &= \underbrace{\begin{pmatrix} G^{0,11} & G^{0,12} & G^{0,13} \\ G^{0,21} & G^{0,22} & G^{0,23} \\ G^{0,31} & G^{0,32} & G^{0,33}\end{pmatrix}}_{\hat{G}^0} + \underbrace{\begin{pmatrix} G^1 & & \\ & 0 & \\ & & 0\end{pmatrix}}_{\hat{G}^1} \\ &+ \underbrace{\begin{pmatrix} 0 & & \\ & G^2 & \\ & & 0\end{pmatrix}}_{\hat{G}^2} + \underbrace{\begin{pmatrix} 0 & & \\ & 0 & \\ & & G^3\end{pmatrix}}_{\hat{G}^3}.\end{aligned} \tag{24}$$

The derivation of the flux spectrum for any given pair of bodies mirrors *exactly* the derivation in Sec. II, with the only difference being the modified SIE matrix W. The final expression for the flux spectrum into V^j due to random currents in $V^{i\neq j}$ is given by

$$\Phi^{ij} = \frac{1}{2\pi}\mathrm{Tr}[(\mathrm{sym}G^i)W^{ji*}(\mathrm{sym}G^j)W^{ji}], \tag{25}$$

which again is invariant under $i \leftrightarrow j$ interchange.

2. Nested bodies

Consider now the system depicted in Fig. 3, involving three bodies at different temperatures with one of the bodies (medium 2) containing another (medium 3). Applying the principle of equivalence again, one finds

$$\begin{aligned}\phi^0 &= \phi^{0+} + \Gamma^0 \star (\xi^1 + \xi^2), \\ \phi^2 &= \phi^{2+} - \Gamma^2 \star (\xi^2 - \xi^3), \\ \phi^r &= \phi^{r+} - \Gamma^r \star \xi^r,\end{aligned}$$

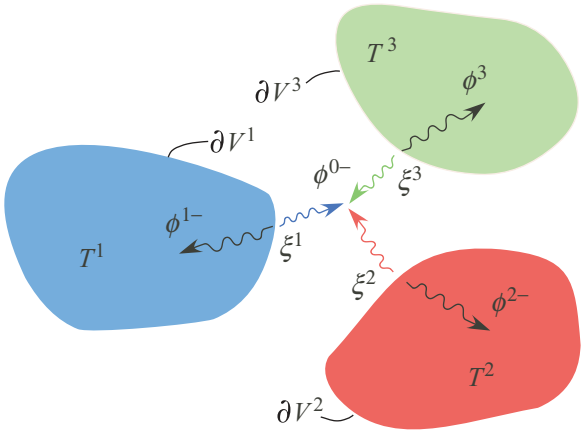

FIG. 2. (Color online) Schematic depicting three disconnected bodies described by surfaces ∂V^1, ∂V^2, and ∂V^3, and held at temperature T^1, T^2, and T^3, respectively. Surface currents ξ^1, ξ^2, and ξ^3, laying on the surfaces of the bodies give rise to scattered fields ϕ^{1-}, ϕ^{2-}, and ϕ^{3-}, respectively, in the interior of the bodies, and scattered field ϕ^{0-} in the intervening medium 0.

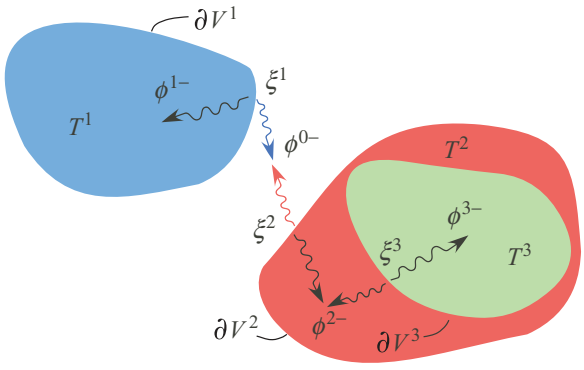

FIG. 3. (Color online) Similar three-body geometry as that depicted in Fig. 2 but with body 3 now embedded in the interior of body 2. Here, the scattered field ϕ^{2-} includes contributions from both ξ^2 and ξ^3.

for $r = 1,3$, with fictitious currents ξ^r determined by the boundary conditions of continuous tangential fields at the body interfaces. Equating the tangential components of the fields at the surfaces of the bodies, one obtains the following integral equations:

$$\begin{aligned}(\Gamma^0+\Gamma^1)\star\xi^1+\Gamma^0\star\xi^2|_{\partial V^1} &= \phi^{1+}-\phi^{0+}|_{\partial V^1},\\ (\Gamma^0+\Gamma^2)\star\xi^2+\Gamma^0\star\xi^1-\Gamma^2\star\xi^3|_{\partial V^2} &= \phi^{2+}-\phi^{0+}|_{\partial V^2},\\ (\Gamma^2+\Gamma^3)\star\xi^3-\Gamma^2\star\xi^2|_{\partial V^3} &= \phi^{3+}-\phi^{2+}|_{\partial V^3},\end{aligned}$$

where ∂V^2 denotes the interface between V^2 and V^0, from which one obtains the corresponding SIE matrix:

$$\begin{aligned}&\underbrace{\begin{pmatrix}W^{11}&W^{12}&W^{13}\\W^{21}&W^{22}&W^{23}\\W^{31}&W^{32}&W^{33}\end{pmatrix}^{-1}}_{W^{-1}}\\ &=\underbrace{\begin{pmatrix}G^{0,11}&G^{0,12}&\\G^{0,21}&G^{0,22}&\\&&0\end{pmatrix}}_{\hat{G}^0}+\underbrace{\begin{pmatrix}G^1&&\\&0&\\&&0\end{pmatrix}}_{\hat{G}^1}\\ &\quad+\underbrace{\begin{pmatrix}0&&\\&G^2&-G^{2,23}\\&-G^{2,32}&G^{2,33}\end{pmatrix}}_{\hat{G}^2}+\underbrace{\begin{pmatrix}0&&\\&0&\\&&G^3\end{pmatrix}}_{\hat{G}^3}.\end{aligned}\tag{26}$$

Although he derivation of the flux spectrum for any given pair of bodies closely mirrors the derivation in Sec. II C, important deviations arise due to the difference in topology. In what follows, we only focus on those steps that differ significantly. The asymmetry of the geometry also means that we must consider Φ for each pair separately.

First, we compute the flux spectrum Φ^{13} into V^3 (the absorbed power in 3) due to dipole current sources in V^1. The flux into body 3 due to a single dipole source σ^1 inside body 1 is given by

$$\begin{aligned}\Phi^{13}_{\sigma^1} &= \tfrac{1}{4}\mathrm{Re}\langle\xi^3,\phi^2\rangle = \tfrac{1}{4}\mathrm{Re}\langle\xi^3,\phi^3\rangle\\ &= \tfrac{1}{4}\mathrm{Re}\langle\xi^3,-\Gamma^3\star\phi^3\rangle\\ &= -\tfrac{1}{4}\mathrm{Re}(x^{3*}G^3x^3).\end{aligned}$$

After ensemble averaging over σ^1 as before, we obtain

$$\Phi^{13} = \frac{1}{2\pi}\mathrm{Tr}[(\mathrm{sym}G^1)W^{31*}(\mathrm{sym}G^3)W^{31}].\tag{27}$$

Second, we compute the flux spectrum Φ^{12} into V^2 (the absorbed power in body 2) due to dipole current sources in V^1. Direct application of Poynting's theorem at ∂V^2 in this case does *not* yield Φ^{12} but rather the quantity we denote as $\Phi^{1(2)}$: the flux into the entire region contained by ∂V^2 from sources in V^1, which includes absorption in both V^2 *and* V^3. It follows that $\Phi^{12} = \Phi^{1(2)} - \Phi^{13}$. So, it only remains to compute $\Phi^{1(2)}$, starting with the flux from a single σ^1 source, given by

$$\begin{aligned}\Phi^{1(2)}_{\sigma^1} &= \tfrac{1}{4}\mathrm{Re}\langle\xi^2,\phi^0\rangle = \tfrac{1}{4}\mathrm{Re}\langle\xi^2,\phi^2\rangle\\ &= \tfrac{1}{4}\mathrm{Re}\langle\xi^2,-\Gamma^2\star(\xi^2-\xi^3)\rangle\\ &= -\tfrac{1}{4}\mathrm{Re}[x^{2*}(G^2x^2-G^{2,23}x^3)],\end{aligned}$$

with the additional x^3 term stemming from absorbed power in body 3. We ensemble average as before and obtain

$$\begin{aligned}\Phi^{12} &= \Phi^{1(2)}-\Phi^{13}\\ &= \frac{1}{2\pi}\mathrm{Tr}[(\mathrm{sym}G^1)W^{21*}(\mathrm{sym}G^2)W^{21}\\ &\quad-(\mathrm{sym}G^1)\mathrm{sym}(W^{21*}G^{2,23}W^{31})]-\Phi^{13}.\end{aligned}\tag{28}$$

Finally, we compute the flux spectrum Φ^{32} into V^2 (the absorbed power in body 2) due to dipole current sources in V^3. Φ^{23} can be computed by subtracting the flux $\Phi^{3(2)}$ leaving body 2 through ∂V^2 from the flux $\Phi^{3(3)}$ entering body 2 through ∂V^3. Specifically, for a single dipole σ^3, we find

$$\begin{aligned}\Phi^{32}_{\sigma^3} &= \tfrac{1}{4}\mathrm{Re}\langle\xi^3,\phi^2\rangle-\tfrac{1}{4}\mathrm{Re}\langle\xi^2,\phi^2\rangle\\ &= \tfrac{1}{4}\mathrm{Re}\langle\xi^3,\phi^3\rangle-\tfrac{1}{4}\mathrm{Re}\langle\xi^2,\phi^2\rangle\\ &= \tfrac{1}{4}\mathrm{Re}\langle\xi^3,-\Gamma^3\star\xi^3\rangle-\tfrac{1}{4}\mathrm{Re}\langle\xi^2,-\Gamma^2\star(\xi^2-\xi^3)\rangle\\ &= \underbrace{-\tfrac{1}{4}\mathrm{Re}(x^{3*}G^3x^3)}_{\Phi^{3(3)}_{\sigma^3}}+\underbrace{\tfrac{1}{4}\mathrm{Re}[x^{2*}(G^2x^2-G^{2,23}x^3)]}_{-\Phi^{3(2)}_{\sigma^3}}.\end{aligned}$$

The final result is the expression

$$\Phi^{32} = \Phi^{3(3)}-\Phi^{3(2)},\tag{29}$$

with

$$\begin{aligned}\Phi^{3(2)} &= \frac{1}{2\pi}\mathrm{Tr}[(\mathrm{sym}G^3)W^{23*}(\mathrm{sym}G^2)W^{23}\\ &\quad+(\mathrm{sym}G^3)\mathrm{sym}(W^{23*}G^{2,23}W^{33})]\end{aligned}\tag{30}$$

$$\Phi^{3(3)} = \frac{1}{2\pi}\mathrm{Tr}[(\mathrm{sym}G^3)W^{33*}(\mathrm{sym}G^3)W^{33}].\tag{31}$$

For example, the heat transfer between V^1 and the combined $V^{(2)} = V^2 \cup V^3$ is given by

$$H^{1(2)} = \int \Theta_{T^1}\Phi^{1(2)}-\Theta_{T^2}\Phi^{12}-\Theta_{T^3}\Phi^{13},\tag{32}$$

where the integral is taken over all positive frequencies ω and $\Theta_T \equiv \Theta(\omega,T)$. In the special case $T^2 = T^3$, the expression reduces to the expected form:

$$H^{1(2)} = \int(\Theta_{T^1}-\Theta_{T^2})\Phi^{1(2)}.\tag{33}$$

As before, we obtain reciprocity relations $\Phi^{ij} = \Phi^{ji}$ between every pair of bodies, but these relations are no longer apparent merely by inspection of Φ^{ij}. Because each body is topologically distinct, Φ^{ji} is no longer obtained from Φ^{ij} merely by interchanging i and j, but instead must be derived separately (using analogous steps). Upon carrying out this derivation, we verify that $\Phi^{ij} = \Phi^{ji}$ as required. Furthermore, the positivity of Φ^{ij} appears harder to derive algebraically from the final expression than in the non-nested cases, and we do not do so in this work. (Although it follows from the second law of thermodynamics, the scattering-matrix proof of positivity[35] should apply to nested bodies with minimal modification.)

IV. VALIDATION

We now apply our FSC formulation to obtain results obtained previously using other scattering formulations in several high-symmetry geometries. In Sec. IV A, we discuss

the choice of basis, contrasting BEMs that use a generic surface mesh with spectral methods that use a Fourier-like basis, and point out that the latter are actually closely related to scattering-matrix methods in the case of high-symmetry geometries. In Sec. IV B, we derive semianalytical expressions of heat radiation and heat transfer for spheres and plates, using surface spherical-harmonics and Fourier bases to describe the SIE surface unknowns, and show that these agree with previous formulas derived using other formulations.[9,34,35,97] In Sec. IV C, we present a general-purpose numerical implementation of the FSC formulation based on a standard triangular-mesh discretization of the surfaces of the bodies known as the BEM "RWG" method; we check it against previous heat-transfer methods by computing the heat transfer between spheres.

A. Choice of basis

The standard approach for solving the SIEs above is to *discretize* them by introducing a finite set of basis functions β_n defined on the surfaces of the bodies. As noted above, an important property of SIE formulations is that β_n is an arbitrary basis of surface vector fields: unlike scattering-matrix formulations,[30–32] they need *not* satisfy any wave equation, nor encapsulate any global information about the scattering geometry, nor consist of "incoming" or "outgoing" waves into or out of the bodies. This lack of restriction on β_n is a powerful property of the SIE formalism.

There are two main categories of basis functions that one could employ: *spectral* bases or *boundary-element* bases. A spectral basis consists of a Fourier-like complete basis of nonlocalized functions, such as spherical harmonics or Chebyshev polynomials,[94] which are truncated to obtain a finite basis. BEMs instead first discretize each surface into a mesh of polygonal *elements* (e.g., triangles) and describe functions piecewise by low-degree polynomials in each element.[24,25,27] Spectral bases have the advantage that they can converge exponentially fast for smooth functions,[94] or in this case for smooth interfaces, but they are not as well suited to handle singularities such as corners, and moreover represent surfaces with essentially uniform spatial resolution. A BEM basis, on the other hand, is more flexible because it can use a nonuniform mesh to concentrate spatial resolution where it is needed,[25,26] and furthermore the localized nature of the basis functions has numerical advantages in assembling and applying the W and G (Green's function) matrices.[98,99] The most common BEM technique employs a mesh of triangular elements (*panels*) with vector-valued polynomial basis functions called an RWG (Rao–Wilson–Glisson) basis,[93] where each basis function is associated with each *edge* of the mesh and is nonzero over a pair of triangles sharing that edge. Many years of research have been devoted to the efficient assembly of the G matrices for the RWG basis (by evaluating the singular panel integrals of Γ),[100–102] and to fast methods for solving the resulting linear equations.[99,103]

For a handful of highly symmetric geometries, however, spectral bases have an additional advantage: a special basis can be chosen such that most of the matrix elements can be computed analytically (and many of the G matrices are diagonal as a consequence of orthogonality). This has a close connection to scattering methods, because whenever there is a known incoming/outgoing wave basis (e.g., spherical waves), one can construct an equivalent set of surface-current basis functions (e.g., spherical harmonics) by the principle of equivalence. (In fact, the principle of equivalence can be used to derive an *exact* equivalence between our Φ expressions and the analogous expressions from the scattering-matrix formulation, which we do not show here.) In the example of interactions between two spherical bodies, if we employ a (vector) spherical-harmonic basis on each body, then the G^r self-interaction matrices are diagonal and the $G^{0,rr'}$ interaction matrix is given by "translation matrices" that relate spherical-wave bases at different origins.[104] In this way, by choosing a geometry-specific basis, the FSC formulation can retain all of the efficiency of the scattering-matrix methods, while preserving the flexibility to employ a different basis as needed.

B. Spectral basis

In this section, we explicitly apply our FSC formulation with a spectral basis in three high-symmetry geometries for which the matrix elements can be evaluated semianalytically: radiation of an isolated plate and an isolated sphere, and heat transfer between two parallel plates. In each case, we reproduce known solutions that were derived previously using scattering-matrix formulations.[9,34,35,97] The main purpose of this section is to illustrate how the FSC formulation with a spectral basis allows semianalytical calculations similar to scattering-matrix formulations (albeit only in the handful of high-symmetry geometries where exact wave solutions can be constructed in each body). To begin with, we review the well-known spectral representation of the homogeneous DGF Γ in bases specialized to particular coordinate systems.

1. Basis of Helmholtz solutions

We wish to work with solutions of Maxwell's equations known analytically within each body and which are orthogonal when evaluated *on the interfaces*. These solutions, evaluated at the interface of each body, will then provide a basis of surface-tangential vector fields in which the G matrices can be evaluated analytically or semianalytically. In particular, we wish to work with solutions $\mathbf{M}$ and $\mathbf{N}$ of the vector Helmholtz equation (equivalent to Maxwell's equations in a homogeneous isotropic medium),[105]

$$(\nabla^2 + k^2)\begin{pmatrix}\mathbf{M}\\ \mathbf{N}\end{pmatrix} = 0, \tag{34}$$

with $\mathbf{M} = -i/k\nabla\times\mathbf{N}$ and $\mathbf{N} = i/k\nabla\times\mathbf{M}$ denoting purely electric and purely magnetic vector fields. [Note that $\mathbf{M}$ and $\mathbf{N}$ come in two flavors, depending on whether on solves Eq. (34) for outgoing or incoming boundary conditions.] Furthermore, we seek solutions of Eq. (34) in a coordinate system that allows separation of variables into "normal" and "tangential" components to some surface ∂V (which is possible for a small number of coordinate systems). We let $\eta_\perp$ represent the separable coordinate identified as the normal coordinate, and let $\boldsymbol{\eta}_\parallel$ represent the remaining tangential coordinates. The choice of coordinate system ultimately corresponds to a choice of basis, or independent solutions labeled by an index n that

correspond to different scattering channels. Specifically, one is led to vector fields:[105]

$$\mathbf{M}_n^{\pm}(\eta_\perp,\boldsymbol{\eta}_\parallel) = \kappa_{n,E}^{\pm}(\eta_\perp)\mathbf{X}_n(\boldsymbol{\eta}_\parallel), \tag{35}$$

$$\mathbf{N}_n^{\pm}(\eta_\perp,\boldsymbol{\eta}_\parallel) = \kappa_{n,M}^{\pm}(\eta_\perp)\mathbf{Z}_n(\boldsymbol{\eta}_\parallel), \tag{36}$$

with $\kappa_n^{\pm}$ and $\{\mathbf{X}_n,\mathbf{Z}_n\}$ denoting the normal and tangential components of the fields and with $\pm$ denoting incoming $(+)$ and outgoing $(-)$ solutions. For example, solutions in spherical coordinates yield the well-known vector spherical-wave solutions $\mathbf{M}_{\ell,m}^{\pm}(r,\theta,\phi) = R_\ell^{\pm}(r)\mathbf{Y}_{\ell,m}(\theta,\phi)$, described by spherical Hankel functions $\kappa_{\ell,m,E}^{\pm} = R_\ell^{\pm}$ and vector spherical harmonics $\mathbf{X}_{\ell,m} = \mathbf{Y}_{\ell,m}$ in terms of radial and angular coordinates $\eta_\perp = r$ and $\boldsymbol{\eta}_\parallel = \{\theta,\phi\}$, respectively, and labeled by angular-momentum "quantum" numbers $n = \{\ell,m\}$.

Because $\mathbf{M}_n$ and $\mathbf{N}_n$ form an orthonormal basis (due to the self-adjointness of the Helmholtz operator), the homogeneous photon DGFs $\mathbb{G}$ and $\mathbb{C}$ of Sec. II A can be expressed in such a basis as[104–106]

$$\mathbb{G}(k;\mathbf{x},\mathbf{x}') = \frac{\eta_\perp(\hat{\mathbf{x}})\eta_\perp(\hat{\mathbf{x}}')}{2ik}\,\delta(\mathbf{x}-\mathbf{x}') + \sum_n \begin{cases} \chi_{n,E}\mathbf{M}_n^+(\mathbf{x})\otimes\mathbf{M}_n^-(\mathbf{x}') + \chi_{n,M}\mathbf{N}_n^+(\mathbf{x})\otimes\mathbf{N}_n^-(\mathbf{x}') & \eta_\perp(\mathbf{x}) > \eta_\perp(\mathbf{x}') \\ \chi_{n,E}\mathbf{M}_n^-(\mathbf{x})\otimes\mathbf{M}_n^+(\mathbf{x}') + \chi_{n,M}\mathbf{N}_n^-(\mathbf{x})\otimes\mathbf{N}_n^+(\mathbf{x}') & \eta_\perp(\mathbf{x}) < \eta_\perp(\mathbf{x}'), \end{cases} \tag{37}$$

and $\mathbb{C} = \frac{i}{k}\nabla\times\mathbb{G}$, respectively, where the coefficients χ_n are determined by taking the Wronskian of the outgoing $(-)$ and incoming $(+)$ solutions.

The SIE matrices appearing in Eq. (18) involve inner products of Eq. (37) with basis functions β_n defined at the *surfaces* of the bodies. (Note that because the Green's functions are evaluated on the surface, inclusion of the delta-function term is crucial.[107] Just as the vector fields $\mathbf{M}_n$ and $\mathbf{N}_n$ form a convenient basis in which to expand waves propagating inside and outside ∂V, so too do the *tangential* components $\mathbf{X}_n$ and $\mathbf{Z}_n$ form a suitable basis in which to express surface-current basis functions β_n defined on ∂V. In this case, as in the case of RWG basis functions,[26] β_n can be chosen to be purely electric (E) or purely magnetic (M), so that

$$\beta_{n,E} = \begin{pmatrix}\mathbf{X}_n\\ 0\end{pmatrix}, \quad \beta_{n,M} = \begin{pmatrix}0\\ \mathbf{Z}_n\end{pmatrix}. \tag{38}$$

Moreover, the orthogonality relations of the tangential vector fields, $\langle\mathbf{X}_m,\mathbf{X}_n\rangle = \langle\mathbf{Z}_m,\mathbf{Z}_n\rangle = \delta_{mn}$ and $\langle\mathbf{X}_m,\mathbf{Z}_n\rangle = 0$, mean that only basis functions with the same n and same polarization have nonzero overlap. These surface currents form a complete basis and satisfy convenient orthogonality relations with the corresponding vector fields:

$$\langle\mathbf{X}_m,\mathbf{M}_n^{\pm}\rangle = (\kappa_{n,E}^{\pm}|_{\partial V})\delta_{mn}, \tag{39}$$

$$\langle\mathbf{Z}_m,\mathbf{N}_n^{\pm}\rangle = (\kappa_{n,M}^{\pm}|_{\partial V})\delta_{mn}, \tag{40}$$

$$\langle\mathbf{X}_m,\mathbf{N}_n^{\pm}\rangle = \langle\mathbf{Z}_m,\mathbf{M}_n^{\pm}\rangle = 0, \tag{41}$$

with inner products $\langle\cdot,\cdot\rangle$ corresponding to surface integrals over the tangential coordinates evaluated at the surface ∂V, i.e., $\langle\varphi,\psi\rangle = \oint\!\!\!\oint_{\partial V} d^2\boldsymbol{\eta}_\parallel\,\mathcal{J}(\eta_\perp,\boldsymbol{\eta}_\parallel)\varphi^*\psi$, where $\mathcal{J}$ denotes the Jacobian factor for the coordinate system.

The combination of these orthogonality relations and the Green's function expression of Eq. (37), implies that the G matrices arising in the SIE formulation for interface ∂V will be diagonal and known analytically in this basis. Therefore choosing this basis simplifies the calculation of Φ, as illustrated in the next sections.

2. *Heat-transfer formulation*

Expression of the homogeneous Green's function in the interior of each high-symmetry body r in the basis specialized for that body yields a block-diagonal self-interaction matrix G^r with matrix elements $G^r_{mn,QQ'} = \langle\beta^r_{m,Q},\Gamma^r\star\beta^r_{n,Q'}\rangle \sim \delta_{mn}$, where Q denotes polarization. In contrast, the lack of any orthogonality relations between wave solutions constructed for different, unrelated bodies means that the interaction matrices $\hat{G}^{0,rr'}$ are dense, i.e., the matrix elements $G^{0,rr'}_{mn,QQ'} = \langle\beta^r_{m,Q},\Gamma^0\star\beta^{r'}_{n,Q'}\rangle$ generally do not vanish. The outgoing fields into the intervening medium $\Gamma^r\star\beta^r_{m,Q}$ due to currents in body r are still known analytically from Eq. (37), described in terms of the wave solutions specialized to body r (albeit evaluated in the exterior medium 0), but in order to take inner products with $\beta^{r'}_{n,Q}$ for a body r' we need to "translate" the solutions centered on r to the different basis of waves centered on $r'\neq r$. Such change of bases are often performed via "translation" and "conversion" matrices that are well-known and tabulated for most shapes of interest,[104] and immediately yield the SIE interaction matrices $G^{0,rr'}$.

For the remainder of the section, we restrict ourselves to situations involving either a single body or two identical bodies described by a common set of basis functions, in which case the individual SIE matrices are block-diagonal in n and polarization. In particular, the G matrices for a given n are given by

$$\hat{G}^0 = \begin{pmatrix} G_\perp^{0,11} & G_\perp^{0,12} & & \\ G_\perp^{0,21} & G_\perp^{0,22} & & \\ & & G_\parallel^{0,11} & G_\parallel^{0,12} \\ & & G_\parallel^{0,21} & G_\parallel^{0,22} \end{pmatrix},$$

$$\hat{G}^1 = \begin{pmatrix} G_\perp^1 & & & \\ & 0 & & \\ & & G_\parallel^1 & \\ & & & 0 \end{pmatrix}, \quad \hat{G}^2 = \begin{pmatrix} 0 & & & \\ & G_\perp^2 & & \\ & & 0 & \\ & & & G_\parallel^2 \end{pmatrix},$$

where $G_\perp$ and $G_\parallel = G_\perp(E\to H)$ are 2×2 block matrices

$$G_{\perp,nn} = \begin{pmatrix} \langle\mathbf{X}_n,\boldsymbol{\Gamma}^{EE}\star\mathbf{X}_n\rangle & \langle\mathbf{X}_n,\boldsymbol{\Gamma}^{EH}\star\mathbf{Z}_n\rangle \\ \langle\mathbf{Z}_n,\boldsymbol{\Gamma}^{HE}\star\mathbf{X}_n\rangle & \langle\mathbf{Z}_n,\boldsymbol{\Gamma}^{HH}\star\mathbf{Z}_n\rangle \end{pmatrix}. \tag{42}$$

Here, the subscripts $\perp$ and $\parallel$ refer to the two decoupled polarization states, corresponding to purely electric E and purely magnetic M surface currents, respectively. The separability of the two polarizations means that the flux spectrum Φ can be written in the form $\Phi = \sum_{\rm p} \Phi_{\rm p}$, with $\Phi_{\rm p}$ denoting the contribution of the p polarization. From the definitions of the Γ functions, it follows that the two are related to one another by $\Phi_\parallel = \Phi_\perp(Z \to 1/Z)$.

In the subsequent sections, we derive semianalytical expressions for Φ in special geometries involving isolated and interacting plates and spheres. The symmetry of these geometries make it convenient to represent the SIE matrices using Fourier and spherical-wave surface basis functions, described in Appendix A. Our final expressions agree with previous formulas derived using the scattering-matrix approach.[9,34,35,97]

3. Isolated plates

We first consider the radiation of an isolated plate. Using the appropriate Fourier basis supplied in Appendix A 1 and the corresponding Green's function expansion of Eq. (37), the $G_\perp$ matrices for the plate are given by

$$G_\perp^{0,11} = \frac{1}{2}\begin{pmatrix} \frac{Z_0}{\gamma_0} & 1 \\ 1 & -\frac{\gamma_0}{Z_0} \end{pmatrix}, \quad G_\perp^{1} = \frac{1}{2}\begin{pmatrix} \frac{Z_1}{\gamma_1} & -1 \\ -1 & -\frac{\gamma_1}{Z_1} \end{pmatrix}, \tag{43}$$

where $\gamma_r = \sqrt{1-(|\mathbf{k}_\perp|/k^r)^2}$ is the wavenumber in the z direction normalized by k^r. It follows that the flux spectra for the two polarizations are given by

$$\begin{aligned} \Phi_\perp &= \frac{1}{4\pi}\mathrm{Tr}\left[\frac{\mathrm{Re}\left(\frac{\gamma_0}{Z_0}\right)\mathrm{Re}\left(\frac{\gamma_1}{Z_1}\right)}{\left|\frac{\gamma_0}{Z_0}+\frac{\gamma_1}{Z_1}\right|^2}\right], \\ \Phi_\parallel &= \Phi_\perp\left(Z \to \frac{1}{Z}\right), \end{aligned} \tag{44}$$

with $\mathrm{Tr}\Phi = \int \frac{d^2\mathbf{k}_\perp}{(2\pi)^2}\,\Phi(\mathbf{k}_\perp)$ corresponding to integration over the parallel wave vector. Assuming a nondissipative external medium ($\mathrm{Im}\varepsilon_0 = \mathrm{Im}\mu_0 = 0$), and performing straightforward algebraic manipulations, one obtains the well-known formula for the emissivity of the plate:[17]

$$\Phi(\omega) = \frac{1}{8\pi}\int_0^\omega \frac{d^2\mathbf{k}_\perp}{(2\pi)^2}\sum_{\mathrm{p}=\{\perp,\parallel\}}\epsilon_{\rm p}(\mathbf{k}_\perp,\omega), \tag{45}$$

where $\epsilon_{\rm p} = \frac{1}{2}(1-|r_{\rm p}|^2)$ denotes the directional emissivity of the plate for the p polarization, expressed in terms of the Fresnel reflection coefficients:[83]

$$r_\perp = \frac{\frac{\gamma_0}{Z_0}-\frac{\gamma_1}{Z_1}}{\frac{\gamma_0}{Z_0}+\frac{\gamma_1}{Z_1}}, \quad r_\parallel = r_\perp\left(Z \to \frac{1}{Z}\right). \tag{46}$$

4. Isolated spheres

We now consider the radiation of an isolated sphere. Using the appropriate vector spherical wave basis supplied in Appendix A 2 and the corresponding Green's function expansion, the $G_\perp$ matrices for the sphere are given by

$$G_\perp^{0,11} = (z_0R)^2\begin{pmatrix} Z_0 j_\ell(z_0)h_\ell(z_0) & i j_\ell(z_0)\breve{h}_\ell(z_0) \\ -i j_\ell(z_0)\breve{h}_\ell(z_0) & \frac{1}{Z_0} j_\ell(z_0)\breve{h}_\ell(z_0) \end{pmatrix}, \tag{47}$$

$$G_\perp^{1} = (z_1R)^2\begin{pmatrix} Z_1 j_\ell(z_1)h_\ell(z_1) & i \breve{j}_\ell(z_1)h_\ell(z_1) \\ -i \breve{j}_\ell(z_1)h_\ell(z_1) & \frac{1}{Z_1} \breve{j}_\ell(z_1)\breve{h}_\ell(z_1) \end{pmatrix}, \tag{48}$$

where $\breve{f}(z) \equiv (1/z + d/dz)f$, j_ℓ and h_ℓ are Bessel functions of the first and second kind, respectively, and $z_r = k^r R$. Employing a number of well-known properties of spherical Bessel functions, such as the Wronskian identity $j'_\ell(z)h_\ell(z) - h'_\ell(z)j_\ell(z) = i/z^2$, one arrives at the following flux spectra for the two polarizations:

$$\Phi_\perp = \frac{1}{8\pi}\mathrm{Tr}\left[\frac{1}{|z_0 h_\ell(z_0)|^2}\frac{\mathrm{Im}\left[\frac{Z_0}{Z_1}\frac{\breve{j}_\ell(z_1)}{j_\ell(z_1)}\right]}{\left|\frac{Z_0}{Z_1}\frac{\breve{j}_\ell(z_1)}{j_\ell(z_1)}-\frac{\breve{h}_\ell(z_0)}{h_\ell(z_0)}\right|^2}\right], \tag{49}$$

$$\Phi_\parallel = \Phi_\perp\left(Z \to \frac{1}{Z}\right), \tag{50}$$

with $\mathrm{Tr}\Phi = \sum_{\ell,m}\Phi_{\ell m}$ corresponding to a sum over the angular-momentum quantum numbers. Assuming vacuum as the external medium ($\varepsilon_0 = \mu_0 = 1$) and a nonmagnetic sphere ($\mu_1 = 1$), one obtains the well-known formula for the emissivity of a sphere in vacuum:[97]

$$\begin{aligned} \Phi(\omega) = \frac{1}{8\pi}\sum_{\ell>1}\frac{(2\ell+1)}{|z_0 h_\ell(z_0)|^2} \\ \times\left[\frac{\mathrm{Im}\left[n_1\frac{\breve{j}_\ell(z_1)}{j_\ell(z_1)}\right]}{\left|n_1\frac{\breve{j}_\ell(z_1)}{j_\ell(z_1)}-\frac{\breve{h}_\ell(z_0)}{h_\ell(z_0)}\right|^2}+\frac{\mathrm{Im}\left[n_1^*\frac{\breve{j}_\ell(z_1)}{j_\ell(z_1)}\right]}{\left|n_1\frac{\breve{h}_\ell(z_0)}{h_\ell(z_0)}-\frac{\breve{j}_\ell(z_1)}{j_\ell(z_1)}\right|^2}\right], \end{aligned} \tag{51}$$

where $n_1 = \sqrt{\varepsilon_1}$ is the index of refraction of the sphere.

5. Two plates

Finally, we consider the heat transfer between two parallel, semi-infinite plates separated by distance d. Just as in the case of isolated plates, it is convenient to express the $G_\perp$ matrices in the Fourier basis supplied in Appendix A 1. Here, in addition to the self-interaction matrices

$$G_\perp^{0,rr} = \frac{1}{2}\begin{pmatrix} \frac{Z_0}{\gamma_0} & 1 \\ 1 & -\frac{\gamma_0}{Z_0} \end{pmatrix}, \quad G_\perp^{r} = \frac{1}{2}\begin{pmatrix} \frac{Z_r}{\gamma_r} & -1 \\ -1 & -\frac{\gamma_r}{Z_r} \end{pmatrix}, \tag{52}$$

for $r = 1,2$, one obtains the interaction or "translation" matrices

$$G_\perp^{12} = G_\perp^{21} = \frac{1}{2}\begin{pmatrix} \frac{Z_0}{\gamma_0} & 1 \\ 1 & \frac{\gamma_0}{Z_0} \end{pmatrix} e^{ik_0\gamma_0 d}, \tag{53}$$

where the exponential factors above couple or "translate" waves arising in different origins. Straightforward matrix algebra yields the following flux spectra for the two polarizations:

$$\Phi_\perp = \frac{1}{2\pi}\mathrm{Tr}\left[\frac{\left|\frac{\gamma_0}{Z_0}e^{2ik_0\gamma_0 d}\right|^2}{|\rho_\perp|^2}\frac{\mathrm{Re}\left(\frac{\gamma_1}{Z_1}\right)\mathrm{Re}\left(\frac{\gamma_2}{Z_2}\right)}{\left|\frac{\gamma_0}{Z_0}+\frac{\gamma_1}{Z_1}\right|^2\left|\frac{\gamma_0}{Z_0}+\frac{\gamma_2}{Z_2}\right|^2}\right], \tag{54}$$

$$\Phi_\parallel = \Phi_\perp\left(Z \to \frac{1}{Z}\right), \tag{55}$$

where $\rho_p = |1 - r_p^1 r_p^2 e^{2ik_0\gamma_0 d}|^2$ and r_p^q is the Fresnel reflection coefficient of plate q for the p polarization given in Eq. (46). Assuming a nondissipative external medium ($\mathrm{Im}\varepsilon_0 = \mathrm{Im}\mu_0 = 0$), and performing straightforward algebraic manipulations, one obtains the well-known formula[17]

$$\Phi(\omega) = \Phi_{\mathrm{prop}}(\omega) + \Phi_{\mathrm{evan}}(\omega), \tag{56}$$

with

$$\Phi_{\mathrm{prop}}(\omega) = \frac{1}{4\pi}\sum_p \int_0^\omega \frac{d^2\mathbf{k}_\perp}{(2\pi)^2}\frac{\epsilon_p^1\epsilon_p^2}{\rho_p}, \tag{57}$$

$$\Phi_{\mathrm{evan}}(\omega) = \frac{1}{4\pi}\sum_p \int_\omega^\infty \frac{d^2\mathbf{k}_\perp}{(2\pi)^2}\left(\mathrm{Im}r_p^1\right)\left(\mathrm{Im}r_p^2\right)\frac{e^{-2\mathrm{Im}(k_0\gamma_0)d}}{\rho_p}, \tag{58}$$

where ϵ_p^q denotes the emissivity of plate q for the p polarization and where Φ has been conveniently decomposed into far-field (propagating) and near-field (evanescently decaying) contributions.

C. BEM discretization via RWG basis

In contrast to spectral methods, BEMs discretize the surfaces of the bodies into polygonal *elements* or "panels," and describe piecewise functions in each element by low-degree polynomials.[25,27] The most common BEM technique employs a so-called RWG basis of vector-valued polynomial functions defined on a mesh of triangular panels.[93] Such a basis is applicable to arbitrary geometries and yields results that converge with increasing resolution (smaller triangles), where variants with different convergence rates depend upon the degree of the polynomials used in the triangles (which can be curved). The simplest discretizations involve degree-1 polynomials and flat triangles, where the error decreases at least linearly with 1/diameter of the triangles, but can converge faster with adaptive mesh refinements.[27] In contrast to spectral methods, the G_{nm} integrals here must be performed numerically and the resulting G matrices are dense, but, thankfully, fast techniques to perform these integrals are well established and need only be implemented once for a given RWG basis, independent of the geometry.[24,25,93] One such implementation is the free-software solver SCUFF-EM,[108] which we exploit in this section to compare results from BEM RWG to known results for spheres; the same code is employed in Sec. V to obtain results in new and more complex geometries.

The heat-transfer rate H between two spheres was recently obtained numerically by Ref. 29. In contrast to scattering-matrix methods or the FSC formalism above, the method of Ref. 29 involves straightforward integration of the inhomogeneous Green's function of the geometry over the volumes of the two spheres, expressed in terms of a specialized spherical-wave basis expansion with coefficients determined by enforcing continuity of the fields across the various interfaces. The result of the integration is an exponentially convergent semianalytical formula of the kind derived in Sec. IV B. Figure 4 compares the results of the BEM RWG method (red circles) against those obtained by evaluating the semianalytical formula of Ref. 29, truncated at a sufficiently large but finite order (solid lines). In particular, the heat-transfer ratio $\mathcal{H} = H/\sigma T^4 A$

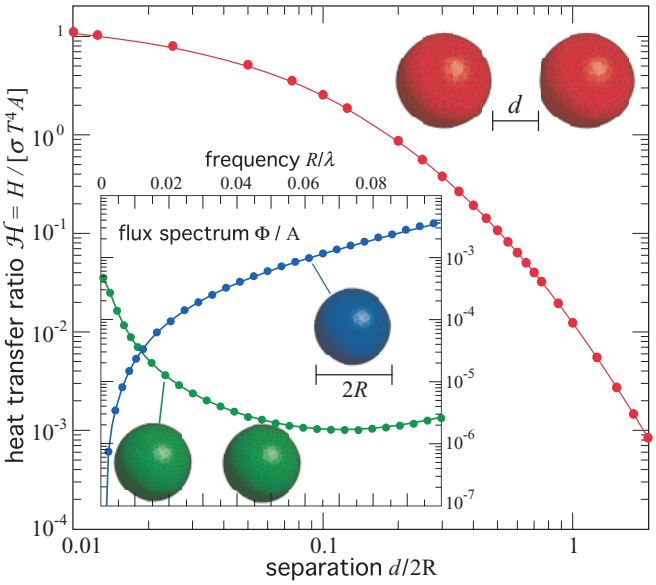

FIG. 4. (Color online) Ratio $\mathcal{H} = H/\sigma T^4 A$ of the heat-transfer rate H between gold spheres of radii $R = 0.2\ \mu$m and the Stefan-Boltzmann law $\sigma T^4 A$, where $A = 4\pi R^2$ is the surface area of the spheres, with one sphere held at $T = 300$ K and the other held at zero temperature, as a function of their surface-surface separation. (Inset) Flux spectra $\Phi(\omega)$ per unit area A (units of μm^2) of the two spheres at $d = R$ (green circles) and of an isolated sphere (blue circles).

is plotted as a function of surface-surface separation d for gold spheres of radius $R = 1\ \mu$m, where one sphere is held at $T = 300$ K, while the other is held at zero temperature, and where $\sigma T^4 A$ is the Stefan-Boltzmann (SB) law (for a planar black body), with $\sigma = \pi^2 k_B^2/(60\hbar^3 c^2)$ and A the surface area of the spheres. The inset of the figure also shows the corresponding flux spectra Φ of both interacting ($d = R$) and isolated spheres, normalized by A and plotted over relevant wavelengths $\lambda \gtrsim \lambda_T$, where $\lambda_T = \hbar c/k_B T \approx 7.6\ \mu$m denotes the thermal wavelength corresponding to the peak of the thermal spectrum. In both cases, the BEM results (circles) are shown to agree with the corresponding semianalytical formulas [in the case of isolated spheres, the flux spectrum is compared against Eq. (51)].

V. APPLICATIONS

In this section, we illustrate the generality and broad applicability of the FSC formulation by applying the BEM RWG method to obtain new results in complex geometries. As discussed above, most calculations of heat transfer have focused primarily on semi-infinite planar bodies.[23] Finite bodies only recently became accessible with the development of sophisticated spectral methods,[30–35,78] albeit for highly symmetric bodies with smooth shapes (e.g., spheres) for which convenient spectral bases exist. Here, we will focus instead on geometries involving finite bodies with sharp corners (combinations of finite plates, cylinders, and cones) that pose no challenge for the BEM RWG method but which prove difficult to model via spectral methods.

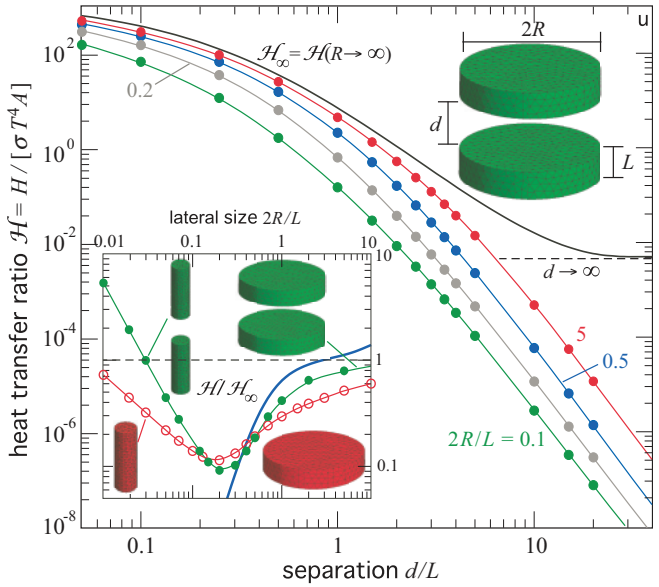

FIG. 5. (Color online) Ratio $\mathcal{H} = H/\sigma T^4 A$ of the heat-transfer rate H from a finite, gold circular plate of lateral size $2R$ and thickness $L = 0.2\ \mu$m held at $T = 300$ K, to an identical plate held at zero temperature, and the SB law $\sigma T^4 A$ (where $A = \pi R^2$ is the "interaction" surface area of the plates), as a function of their surface-surface separation d. $\mathcal{H}$ is plotted for multiple aspect ratios $2R/L$ (circles). The solid black line corresponds to the heat-transfer ratio $\mathcal{H}_\infty = \mathcal{H}_\infty(R\to\infty)$ obtained upon taking the limit $R\to\infty$, which is computed via the semianalytical formula in Ref. 109. (Inset) Heat-transfer rate between two plates at a fixed separation $d = 0.1L$ (solid circles) and heat radiation of an isolated plate (open circles) or sphere (thick solid line) as a function of lateral size or diameter.

A. Plates and cylinders

To begin with, we extend the calculation of heat transfer between planar semi-infinite plates to the case of finite plates, which quantifies the influence of lateral size effects in that geometry. Figure 5 shows the ratio $\mathcal{H} = H/\sigma T^4 A$ of the heat-transfer rate H between finite circular plates of thickness L and lateral size $2R$ and the SB law, with one plate held at $T = 300$ K and the other held at zero temperature as a function of their surface-surface separation d. $\mathcal{H}$ is plotted for multiple aspect ratios $2R/L$ (solid circles), with fixed $L = 0.2\ \mu$m. For comparison, we also plot the heat-transfer ratio $\mathcal{H}_\infty$ for semi-infinite ($R\to\infty$) plates of the same thickness (black solid line), which is obtained analytically from the absorptivity of the plates via Kirchhoff's law of thermal radiation.[4,110] As expected, one finds that at small d, near-field effects dominate and $\mathcal{H}\sim 1/\sqrt{d}$ for both finite and semi-infinite plates. In contrast, at asymptotically large d, the finite plates behave like dipoles and one finds that $\mathcal{H}\sim 1/d^5$, whereas the semi-infinite transfer rate approaches a constant $\mathcal{H}_\infty(d\to\infty) \ll 1$ independent of d; the rate is significantly smaller than that of a perfect black body because gold is highly reflective. As $R\to\infty$, the BEM results approach $\mathcal{H}_\infty$ for all separations d, albeit at different rates, where smaller separations converge faster than larger separations.

To quantify finite-size effects, the inset of Fig. 5 shows $\mathcal{H}/\mathcal{H}_\infty$ for isolated and interacting plates (at a single separation $d = 0.1L$) as a function of R. As above, in the limit of large $R \gg \lambda_T \gg L$, such that the dominant wavelengths and corresponding skin depths $\delta = c/\mathrm{Im}\sqrt{\varepsilon}\omega$ are much smaller than the lateral dimensions of the plates, $\mathcal{H}\to\mathcal{H}_\infty$. In the case of isolated plates, the relevant length scales are λ_T and δ, whereas in the case of interacting plates, the separation d also factors into the convergence rate: the increasing contribution of (long-wavelength) near-field effects to the heat transfer at smaller separations means that smaller separations converge faster to the $\mathcal{H}_\infty$ result than larger separations. (For the particular separation $d = 0.1L$ plotted here, near-field effects are large enough to cause the convergence rate of the interacting plates to be significantly larger than that of the isolated plate.) At intermediate $R \lesssim L \ll \lambda_T$, the plates no longer resemble plates but rather elongated cylinders, leading to significant deviations in $\mathcal{H}$.

Compared to the heat radiation of semi-infinite cylinders ($L/R\to\infty$ for fixed R), studied previously by Ref. 34, the radiation of finite cylinders displays a number of interesting features. (Note that $\mathcal{H}$ here includes radiation emitted in both the axis-parallel, $\mathcal{H}_\parallel$, and axis-perpendicular, $\mathcal{H}_\perp$, directions.) First, due to the finite value of L, in the limit $R\to\infty$, the radiation of our finite cylinders is best characterized by the radiation of thin plates with $\mathcal{H}_\parallel \gg \mathcal{H}_\perp$. Not surprisingly, we find that $\mathcal{H}\to\mathcal{H}_\infty$ from below as $R\to\infty$, in contrast to what is observed in the semi-infinite case where $\mathcal{H}_\infty$ is approached from above.[34] Second and most interestingly, we find that below a critical R, determined by the smallest skin-depth $\delta \approx 20$ nm of Au over the relevant thermal wavelengths, the radiation normalized by surface area *increases* with decreasing R, leading to nonmonotonicity. Such behavior is unusual in that in this $R \lesssim \delta$ regime, bodies most often behave like volume emitters, causing H to grow with the volumes rather than surfaces of the bodies (as observed in the case of semi-infinite cylinders).[34] Indeed, we find that for dielectric bodies with small and positive ε, one obtains the usual volume dependence of H. In contrast, the enhancement in Fig. 5 arises because for small R, the cylinders act as metallic dipole emitters, whose radiation is increasingly dominated by $\mathcal{H}_\parallel$ as $R\to 0$ and whose quasistatic (long wavelength) parallel polarizability grows with decreasing R (a consequence of the increasing anisotropy of the cylinder and large $\mathrm{Im}\varepsilon$).[111,112] For sufficiently small R, the heat transfer per unit area of the uniaxial cylinders can greatly exceed that of the semi-infinite plate, i.e., $\mathcal{H} \gg \mathcal{H}_\infty$. (The dipole model also predicts that $\mathcal{H}$ will eventually vanish as $R\to 0$, but only at radii too small to be easily calculated by BEM. We intend to explore these phenomena more fully in subsequent work.)

It is also interesting to study the convergence of the cylinder radiation rate with L, comparing our results against the semianalytical results obtained in the special case of semi-infinite ($L\to\infty$) cylinders.[34] We also consider the heat transfer between nonuniaxial (parallel) cylinders. Figure 6 shows the flux spectra Φ of isolated cylinders of radius $R = 0.2\ \mu$m and varying lengths L; for comparison, we also plot the spectrum of the semi-infinite cylinders[34] (solid lines). As before, Φ is normalized by the surface area A of each object. (For the relevant wavelength range shown in the figure, R is several times δ, which means that most of the radiation is coming from sources near the surface of the objects.[34]) We find that for $L/R \approx 2$ (not shown), corresponding to

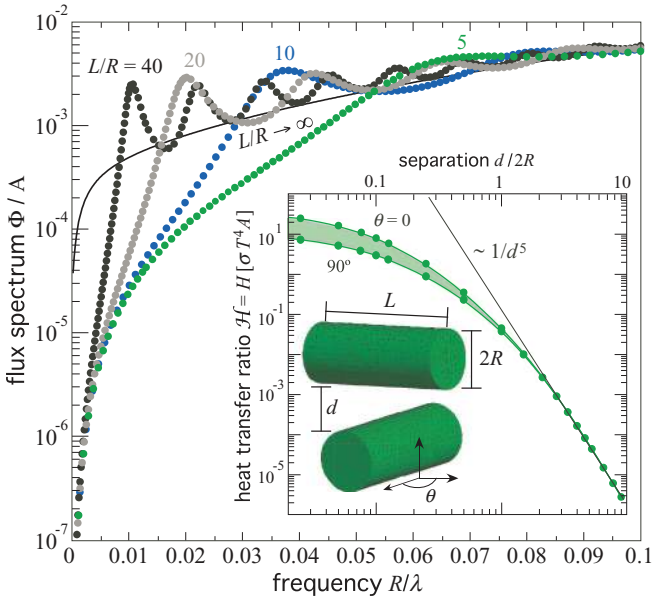

FIG. 6. (Color online) Flux spectrum $\Phi(\omega)$ of an isolated gold cylinder of length L and radius $R = 0.2\ \mu$m normalized by its corresponding surface area A and plotted for multiple aspect ratios L/R (solid circles). The solid line shows Φ in the limit $L \to \infty$ of a semi-infinite cylinder, as computed by the semianalytical formula of Ref. 34. (Inset) Heat-transfer ratio $\mathcal{H}$ of heat transfer H from a room-temperature cylinder of aspect ratio $L/R = 5$ to an identical cylinder at zero temperature, and the SB law $\sigma T^4 A$, with $A = 2\pi R(R + L)$ denoting the total surface area of each cylinder, as a function of their surface-surface separation d. H is plotted for both parallel ($\theta = 0$) and crossed ($\theta = 90^\circ$) cylinder configurations, with the shaded region corresponding to intermediate θ.

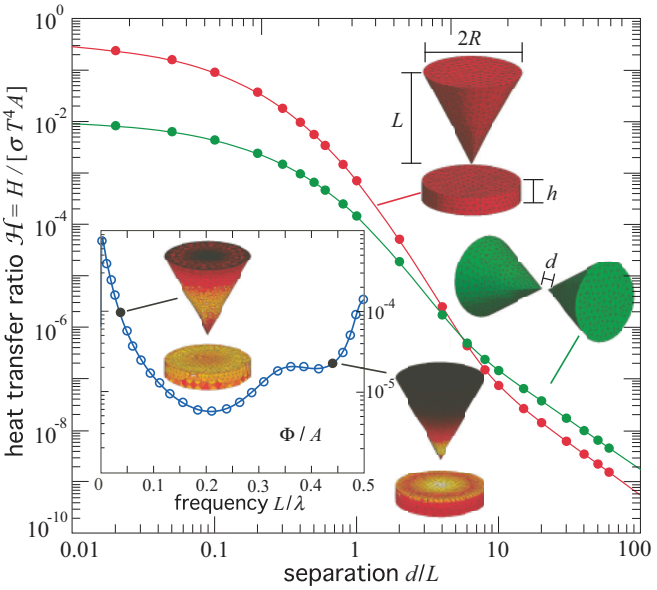

FIG. 7. (Color online) Heat-transfer rate H from a room-temperature gold cone of base radius $R = 1\ \mu$m and length $L = 2R$, to either an identical cone (green circles) or a gold plate of radius R and thickness $h = 0.2\ \mu$m, held at zero temperature, as a function of their surface-surface separation d. H is normalized by the Stefan-Boltzmann law $\sigma T^4 A$, where A is the surface area of the cone. (Inset) Flux spectrum $\Phi(\omega)$ of the cone-plate configuration at a single separation $d = 0.2L$, normalized by the area of the cone. The two surface-contour plots show the distribution of flux pattern on the surfaces of the bodies at two wavelengths, $\lambda \approx 30L$ and $\approx 2.2L$, where white/black denotes the maximum/minimum flux at the corresponding wavelength.

nearly isotropic cylinders, Φ is only slightly larger than that of an isolated sphere due to the small but non-negligible contribution of volume fluctuations to Φ. As L/R increases, Φ increases over all λ, and converges towards the $L \to \infty$ limit (black solid line) as $\lambda \to 0$, albeit slowly. Moreover, $\Phi_L \gg \Phi_\infty$ at particular wavelengths, a consequence of *geometrical* resonances that are absent in the semi-infinite case—away from these resonances, Φ clearly straddles the $L \to \infty$ result so long as $\lambda \lesssim L$. As in the case of finite plates, the Φ of interacting cylinders exhibits significant enhancement at large λ due to near-field effects, so that $\mathcal{H} \to \infty$ with decreasing separation d. The enhancement is evident in Fig. 6, which shows $\mathcal{H}$ over a wide range of d for both parallel- ($\theta = 0$) and crossed-cylinder ($\theta = 90^\circ$) configurations, with one cylinder held at $T = 300$ K and the other at zero temperature (both cylinders have aspect ratio $L/R = 5$). We find once again that there are two very distinct separation regimes of heat transfer: at large $d \gg R$, the cylinders act like dipole emitters and $\mathcal{H}/\mathcal{H}_\infty \sim 1/d^5 \ll 1$ whereas at small $d \ll R$, flux contributions from evanescent waves dominate and $\mathcal{H}/\mathcal{H}_\infty \sim 1/\sqrt{d} \gg 1$. Comparing the heat transfer H in the parallel and crossed-cylinder configurations, we find that $H_\parallel/H_\perp \approx 1$ at large $d \gg R$ but increases significantly at smaller $d \ll R$, again due to near-field effects: in the $d \to 0$ limit, H is dominated by the closest surface-surface interactions, so $H_\parallel/H_\perp \sim L/R \to 5$. As expected, $H_\parallel/H_\perp \to \infty$ as $L \to \infty$ because the increased "interaction" area in this limit favors the parallel over the crossed configuration. Specifically, whereas H grows linearly with L in the parallel configuration, it grows sublinearly (and asymptotes to a finite value in the $L \to \infty$ limit) in the crossed configuration due to the diminishing contributions of near-field and radiative fluxes between surface elements in the extremities of the cylinders.

B. Cones

Finally, motivated by recent predictions,[69] we consider the heat transfer between finite cones and plates. In Ref. 69, the cone-plate geometry (with a semi-infinite plate) was obtained using a "hybrid" scattering-BEM method[69] based on the scattering-theory formulation of Ref. 32. (In contrast to semi-infinite plates or spheres, the scattering-matrix of a cone cannot be easily obtained analytically, and was instead computed numerically by exploiting the BEM method in combination with a multipole basis of cylindrical waves.) Here, in addition to extending these predictions to the case of finite plates, we consider the heat-transfer rate between two oppositely oriented cones. Figure 7 shows the heat-transfer rate h (as in the previous section, $h = H/\sigma T^4 A$ where here $A = \pi R^2$ is the projected area of the cone) from a cone of radius $R = 0.5\ \mu$m and length $L = 2R$ to either an identical cone rotated by 180° (green circles) or a plate of radius R and thickness $L = 0.2\ \mu$m (red circles), as a function of their surface-surface separation d. As before, we consider

gold bodies, with one held at 300 K, while the other is held at zero temperature Similar to Ref. 69, we find that the heat-transfer rate $H \sim \ln(d)$ varies logarithmically with d at short separations $d \ll L \ll \lambda_T$, a consequence of near-field interactions and the finite size of the cone.[113] While h exhibits similar scaling with d for both geometries, h turns out to be almost two orders of magnitude smaller at small $d \ll L$ in the cone-cone geometry, as would be expected from a proximity-approximation (PA) model.[114] The situation is reversed at large separations $d \gg \lambda_T \gg L$: beyond a critical $d \approx 7L$, the cone-cone heat transfer becomes larger than the cone-plate transfer. The reversal is expected on the basis that at these separations, the two bodies act like fluctuating dipoles oriented mainly along their largest dimension (along the axis of symmetry for the cone and along the lateral dimension for the plate), in which case the cone-plate interaction resembles the interaction of two orthogonal dipoles whereas the cone-cone interaction resembles the interaction of two parallel dipoles. Another interesting feature of the heat transfer in this geometry is that the spatial distribution of pattern over the plate exhibits a local minimum directly below the tip of the cone, a consequence of the dipolar field induced on the cone at long wavelengths.[69] Here, we observe a similar phenomenon, but we find that the finite size of the plate significantly alters the scope of the anomalous radiation pattern. In particular, whereas Ref. 69 found this effect to persist over a wide range of wavelengths (surviving even in the total or integrated radiation pattern), we find that in the finite-plate case, it disappears much more rapidly with decreasing wavelength.

VI. CONCLUSION

The FSC approach to nonequilibrium fluctuations presented here permits the study of heat transfer between bodies of arbitrary shape, paving the way for future exploration of heat exchange in microstructured geometries that until now remain largely unexplored in this context. Our formulation shares many properties with previous scattering-matrix formulations of radiative heat transfer, e.g., our final expressions involve traces of matrices describing scattering unknowns, but differs in that our "scattering unknowns" are surface currents defined on the surfaces of the bodies rather than incident and outgoing waves propagating into and out of the bodies.[29–38] As argued above, this choice of description has important conceptual and numerical implications: it allows direct application of the surface-integral equation formalism as well as the boundary-element method. When specialized to handle high-symmetry geometries using special functions that exploit those symmetries, our approach can be used to obtain fast-converging semianalytical formulas in the spirit of previous work based on spectral methods.[32,34,35] Moreover, it can also be applied as a brute-force method, taking advantage of existing, well-studied, and sophisticated BEM codes (with no modifications), to obtain results in arbitrary/complex geometries.

While the main focus of this work was on exploring some of the ways in which the FSC formulation can be applied to study nonequilibrium heat transfer, we believe that analogous techniques can be used to derive corresponding FSC approaches to other fluctuation phenomena, including near-field fluorescence,[115] quantum noise in lasers,[116] and nonequilibrium Casimir forces,[32,117] an idea we plan to explore in future work. Furthermore, although our calculations here focused on geometries involving compact bodies, the same heat-transfer formulas derived above apply to geometries involving infinitely extended/periodic bodies (of importance in applications of heat transfer to thermophotovoltaics). Modifying BEM solvers to handle periodic structures, however, is nontrivial,[118–122] and we therefore consider that case in a subsequent publication.

Finally, although Eq. (18) is already well-suited for efficient numerical implementation, its computational efficiency may be improved by adopting a modified formulation in which the dense G matrices are replaced by certain *sparse* matrices involving overlap integrals among basis functions. In addition to reducing the computational cost of the trace in Eq. (18), this approach has the advantage of allowing the computation of other fluctuation-induced quantities such as nonequilibrium Casimir forces and torques. This alternative formulation will be discussed in a forthcoming publication.

ACKNOWLEDGMENTS

This work was supported by DARPA Contract No. N66001-09-1-2070-DOD, by the AFOSR Multidisciplinary Research Program of the University Research Initiative (MURI) for Complex and Robust On-chip Nanophotonics, Grant No. FA9550-09-1-0704, and by the US Army Research Office under contracts W911NF-07-D-0004 and W911NF-13-D-0001.

APPENDIX A: EIGENFUNCTIONS OF THE HELMHOLTZ EQUATION

In this section, we provide and exploit the standard Fourier and spherical-wave eigenfunctions of the vector Helmholtz operator, obtained by solving Eq. (34) in planar and spherical coordinates,[104,105] to obtain the coefficients χ and κ appearing in the Green's function expansion and orthogonality relations of Eqs. (37), (39), and (41), respectively.

1. Fourier basis

In planar geometries, described by normal and tangential coordinates z and $\mathbf{x}_\perp$, respectively, the eigenfunctions of the Helmholtz operator, labeled by Fourier wave vectors $\mathbf{k}_\perp$ perpendicular to the $\hat{\mathbf{z}}$ axis, are given by

$$\mathbf{M}^{\pm}_{\mathbf{k}_\perp k_z}(z,\mathbf{x}_\perp) = \phi^{\pm}(k_z z)\mathbf{X}_{\mathbf{k}_\perp}(\mathbf{x}_\perp),$$

$$\mathbf{N}^{\pm}_{\mathbf{k}_\perp k_z}(z,\mathbf{x}_\perp) = \phi^{\pm}(k_z z)\left[\mp\frac{k_z}{k}\mathbf{Z}_{\mathbf{k}_\perp}(\mathbf{x}_\perp) + \frac{|\mathbf{k}_\perp|}{k}e^{i\mathbf{k}_\perp\cdot\mathbf{x}}\hat{\mathbf{z}}\right],$$

where $\phi^{\pm}_{\mathbf{k}_\perp k_z} = \frac{1}{|\mathbf{k}_\perp|}e^{i\mathbf{k}_\perp\cdot\mathbf{x}_\perp \pm ik_z z}$, $k_z = \sqrt{k^2 - |\mathbf{k}_\perp|^2}$, and where the tangential fields $\mathbf{X}_{\mathbf{k}_\perp}$ and $\mathbf{Z}_{\mathbf{k}_\perp} = \hat{\mathbf{z}} \times \mathbf{X}_{\mathbf{k}_\perp}$ are

$$\mathbf{X}_{\mathbf{k}_\perp}(\mathbf{x}_\perp) = \frac{i}{|\mathbf{k}_\perp|}(\hat{\mathbf{z}} \times \mathbf{k}_\perp)e^{i\mathbf{k}_\perp\cdot\mathbf{x}_\perp}, \tag{A1}$$

$$\mathbf{Z}_{\mathbf{k}_\perp}(\mathbf{x}_\perp) = \frac{i\mathbf{k}_\perp}{|\mathbf{k}_\perp|}e^{i\mathbf{k}_\perp\cdot\mathbf{x}_\perp}. \tag{A2}$$

The precise form of the Fourier functions $\phi^{\pm} = e^{\pm ik_z z}$ depends on whether one desires a solution involving outgoing (+) or incoming (−) fields, or equivalently, fields propagating away

or toward the origin. The corresponding χ and κ coefficients appearing in the Green's function expansion and orthogonality relations are given by

$$\kappa^{\pm}_{\mathbf{k}_\perp,k_z,E}(z) = \phi^{\pm}(k_z z), \tag{A3}$$

$$\kappa^{\pm}_{\mathbf{k}_\perp,k_z,M}(z) = \mp\gamma\phi^{\pm}(k_z z), \tag{A4}$$

$$\chi_{\mathbf{k}_\perp,k_z} = \frac{i}{2k_z}, \tag{A5}$$

with $\gamma \equiv k_z/k = \sqrt{1-|\mathbf{k}_\perp|^2/(\varepsilon\mu\omega^2)}$.

2. Spherical multipole basis

In spherically symmetric geometries, described by normal and tangential coordinates r and $\{\theta,\phi\}$, respectively, the eigenfunctions of the Helmholtz operator, labeled by angular-momentum quantum numbers ℓ and m, are given by

$$\mathbf{M}^{\pm}_{\ell m}(r,\theta,\phi) = R^{\pm}_\ell(kr)\mathbf{X}_{\ell m}(\theta,\phi),$$

$$\mathbf{N}^{\pm}_{\ell m}(r,\theta,\phi) = \breve{R}^{\pm}_\ell(kr)\mathbf{Z}_{\ell m} + \frac{\ell(\ell+1)}{r}R^{\pm}_\ell(kr)Y_{lm}(\theta,\phi)\hat{\mathbf{r}},$$

where $R^{\pm}_\ell$ and $Y_{\ell m}$ denote spherical Hankel functions and spherical harmonics,[83] respectively, and where the tangential fields $\mathbf{X}_{\ell m} = -\frac{1}{\sqrt{\ell(\ell+1)}}(\hat{\mathbf{r}}\times\nabla)Y_{\ell m}$ and $\mathbf{Z}_{\ell m} = \hat{\mathbf{r}}\times\mathbf{X}_{\ell m}$ are

$$\mathbf{X}_{\ell m}(\theta,\phi) = \frac{1}{\sqrt{l(l+1)}}\left[\frac{im}{\sin\theta}Y_{\ell m}\hat{\theta} - \frac{\partial Y_{\ell m}}{\partial\theta}\hat{\varphi}\right],$$

$$\mathbf{Z}_{\ell m}(\theta,\phi) = \frac{1}{\sqrt{l(l+1)}}\left[\frac{\partial Y_{\ell m}}{\partial\theta}\hat{\theta} + \frac{im}{\sin\theta}Y_{\ell m}\hat{\varphi}\right].$$

Above, we defined $\breve{f}(z) \equiv (1/z + d/dz)f$ for brevity. The precise form of the spherical Bessel radial function

$$R^{\pm}_\ell = \begin{cases} h^{(1)}_\ell & +, \\ j_\ell & -, \end{cases}$$

depends on whether one desires a solution corresponding to outgoing $(+)$ or incoming $(-)$ waves toward the origin, or equivalently, a solution that is well behaved at the origin or at infinity. The χ and κ coefficients appearing in the Green's function expansions and orthogonality relations are given by

$$\kappa^{\pm}_{\ell,m,E}(r) = r^2 R^{\pm}_\ell(kr), \tag{A6}$$

$$\kappa^{\pm}_{\ell,m,M}(r) = ir^2\breve{R}^{\pm}_\ell(kr), \tag{A7}$$

$$\chi_{lm} = ik. \tag{A8}$$

APPENDIX B: EQUIVALENCE PRINCIPLE

In this section, we provide a compact derivation and review of the equivalence principle of classical electromagnetism (closely related to Huygens's principle[88]), which expresses scattered waves in terms of fictitious equivalent currents in a homogeneous medium replacing the scatterer.[24] The equivalence principle is usually derived in a somewhat cumbersome way from a Green's-function approach,[24,89] but a much shorter proof can be derived from the differential form of Maxwell's equation. Understanding this result is central to our FSC formulation of heat transfer.

As before, we restrict ourselves to linear media for which Maxwell's equations can be written as

$$\underbrace{\begin{pmatrix} & \nabla\times \\ -\nabla\times & \end{pmatrix}}_{M}\underbrace{\begin{pmatrix}\mathbf{E}\\ \mathbf{H}\end{pmatrix}}_{\phi} = \frac{\partial}{\partial t}\left[\phi + \chi\star\phi\right] + \underbrace{\begin{pmatrix}\mathbf{J}\\ \mathbf{K}\end{pmatrix}}_{\xi}, \tag{B1}$$

with $\chi\star$ denoting convolution with a 6×6 susceptibility tensor

$$\chi = \begin{pmatrix}\varepsilon - 1 & \\ & \mu - 1\end{pmatrix}.$$

Consider an arbitrary incident wave ϕ, which solves the *source-free* Maxwell's equations in some χ medium with *no* current sources: $M\phi = \frac{\partial}{\partial t}(\phi + \chi\star\phi)$. The equivalence principle states that given any arbitrary but *finite* domain V, one can always choose an *equivalent* surface current ξ that generates the same incident field ϕ in V. To show that such a surface current exists, define the field

$$\tilde{\phi} = \begin{cases}\phi & \in V, \\ 0 & \text{elsewhere.}\end{cases} \tag{B2}$$

It follows that $\tilde{\phi}$ satisfies the source-free Maxwell's equations in *both* the interior and exterior regions—the only question is what happens at the interface ∂V. In particular, the discontinuity of $\tilde{\phi}$ at ∂V produces a surface δ function $\delta_{\partial V}$ in the spatial derivative $M\tilde{\phi}$, and so in order to satisfy Maxwell's equations with this $\tilde{\phi}$, one must introduce a matching δ function, a *surface current* ξ, on the right-hand side. [Here, $\delta_{\partial V}$ is the distribution such that $\iiint \delta_{\partial V}\phi(\mathbf{x}) = \oiint_{\partial V}\phi(\mathbf{x})$ for any continuous test function f.] Specifically, letting $\mathbf{n}$ be the unit inward-normal vector,[123] only the normal derivative $\mathbf{n}\cdot\nabla$ contains a δ function (whose amplitude is the magnitude of the discontinuity), which implies a surface current:

$$\xi = (\Theta\phi)\delta_{\partial V} = \begin{pmatrix}\mathbf{n}\times\mathbf{H} \\ -\mathbf{n}\times\mathbf{E}\end{pmatrix}\delta_{\partial V}, \tag{B3}$$

where Θ is the real-symmetric unitary 6×6 matrix:

$$\Theta = \begin{pmatrix} & \mathbf{n}\times \\ -\mathbf{n}\times & \end{pmatrix} = \Theta^{-1} = \Theta^{\mathrm{T}} = \Theta^{*}. \tag{B4}$$

That is, there is a surface *electric* current given by the surface-tangential components $\mathbf{n}\times\mathbf{H}$ of the incident *magnetic* field, and a surface *magnetic* current given by the components $-\mathbf{n}\times\mathbf{E}$ of the incident *electric* field. These are the equivalent currents of the principle of equivalence (derived traditionally from a Green's function approach[24,89] and from which Huygens's principle is derived[88]).

1. Application to surface integral equations

The equivalence principle is of fundamental importance to SIE formulations of EM scattering. Consider two regions 0 and 1, described by volumes V^0 and V^1 and susceptibilities χ^0 and χ^1, respectively, separated by an interface ∂V^1. As before, one can express the total fields $\phi^r = \phi^{r+} + \phi^{r-}$ in each region r in terms of incident ϕ^{r+} and scattered ϕ^{r-} fields. The principle of equivalence describes an equivalent, fictitious

problem, involving fields

$$\tilde{\phi} = \begin{cases} \phi^0 & \in V^0, \\ 0 & \text{elsewhere,} \end{cases}$$

and surface currents $\xi = \Theta\phi^0 = \Theta\phi^1$ at the ∂V^1 interface, where the second equality follows from continuity of the tangential fields. Since $\tilde{\phi} = 0$ in V^1, it follows that one can replace χ^1 with any other local medium and yet $\tilde{\phi}$ still satisfies Maxwell's equations. In particular, replacing χ^1 with χ^0 implies that one can write the scattered field $\phi^{0-} = \Gamma^0 \star \xi$ in V^0 as the field produced by the same fictitious surface currents ξ in an *infinite* medium 0, with Γ^0 denoting the *homogeneous-medium* Green's function of the infinite medium.

A similar argument applies if one is interested in the field in medium 1, except that the sign of the fictitious currents is reversed to $-\xi$ in order to account for the direction of the discontinuity in going from 1 to 0 in this case. In particular, one can write the scattered field $\phi^{1-} = -\Gamma^1 \star \xi$ in V^1 as the field produced by a fictitious surface current $-\xi$ in an infinite medium 1.

APPENDIX C: RECIPROCITY AND DEFINITENESS

In this section, we present a brief review of the reciprocity relations and definiteness (positivity) properties of the DGF, Γ, connecting surface currents ξ to fields $\phi = \Gamma \star \xi$, in dissipative media, and explain how these relate to corresponding properties of the SIE matrices above (crucial to our derivation of heat transfer in Sec. II). Although for our purposes we need only prove reciprocity and definiteness of the *homogeneous* Green's function (trivial to show in that case since the homogeneous DGF is known analytically), here we consider the more general case of inhomogeneous media. Reciprocity is well known[82,124–127] and positivity follows from general physical principles (currents always do nonnegative work in passive materials[83,84,110,125]), but our goal here is to derive them using the same language employed in our derivations above. More specifically, we explain the source of the sign-flip matrices $\mathcal{S}$ and S, which often go unmentioned because many authors consider only 3×3 Green's functions (relating currents to fields of the same type).

1. Green's functions

It is actually easier to derive the reciprocity and definiteness properties of Γ from the properties of $L = (\Gamma\star)^{-1}$, the Maxwell operator that connects fields ϕ to currents $\xi = L\phi$, because L is a partial-differential operator that can be written down explicitly starting from the (frequency-domain) Maxwell equations $\nabla \times \mathbf{E} = i\omega\mu\mathbf{H} - \mathbf{M}$, $\nabla \times \mathbf{H} = -i\omega\varepsilon\mathbf{E} + \mathbf{J}$, in terms of the permittivity $\varepsilon(\mathbf{x},\omega)$ and permeability $\mu(\mathbf{x},\omega)$ tensors and electric $\mathbf{J}$ and magnetic $\mathbf{M}$ currents. Specifically, the Maxwell operator

$$L = \begin{pmatrix} i\omega\varepsilon & \nabla\times \\ -\nabla\times & i\omega\mu \end{pmatrix} \tag{C1}$$

is neither complex-symmetric, Hermitian, antisymmetric, nor anti-Hermitian in general. Using our previous definition of the inner product:

$$\begin{aligned} \langle\phi,\phi'\rangle &= \int \phi^*\phi' \\ &= \left\langle \begin{pmatrix} \mathbf{E} \\ \mathbf{H} \end{pmatrix}, \begin{pmatrix} \mathbf{E}' \\ \mathbf{H}' \end{pmatrix} \right\rangle = \int \mathbf{E}^* \cdot \mathbf{E}' + \mathbf{H}^* \cdot \mathbf{H}', \end{aligned}$$

it follows that the *off*-diagonal part of L is anti-Hermitian:

$$\begin{aligned} &\left\langle \begin{pmatrix} \mathbf{E} \\ \mathbf{H} \end{pmatrix}, \begin{pmatrix} & \nabla\times \\ -\nabla\times & \end{pmatrix} \begin{pmatrix} \mathbf{E}' \\ \mathbf{H}' \end{pmatrix} \right\rangle \\ &= \int \mathbf{E}^* \cdot \nabla \times \mathbf{H}' - \mathbf{H}^* \cdot \nabla \times \mathbf{E}' \\ &= \int (\nabla \times \mathbf{E}^*) \cdot \mathbf{H}' - (\nabla \times \mathbf{H})^* \cdot \mathbf{E}' \\ &= \left\langle - \begin{pmatrix} & \nabla\times \\ -\nabla\times & \end{pmatrix} \begin{pmatrix} \mathbf{E} \\ \mathbf{H} \end{pmatrix}, \begin{pmatrix} \mathbf{E}' \\ \mathbf{H}' \end{pmatrix} \right\rangle, \end{aligned}$$

where we have used the self-adjointness of $\nabla\times$ and assumed boundary conditions such that the $\oint\!\!\!\!\!\!\int \mathbf{E}^* \times \mathbf{H}' + \mathbf{E}' \times \mathbf{H}^*$ boundary terms at infinity (from the integration by parts) vanish. This is commonly attained by assuming loss in the materials so that the fields decay exponentially at infinity (assuming localized sources), or by imposing outgoing-radiation boundary conditions on $\Gamma\star$ at infinity.[83]

Instead, reciprocity relations are normally derived for the *unconjugated* inner product:

$$\begin{aligned} (\phi,\phi') &= \int \phi^{\mathrm{T}}\phi' = \left(\begin{pmatrix} \mathbf{E} \\ \mathbf{H} \end{pmatrix}, \begin{pmatrix} \mathbf{E}' \\ \mathbf{H}' \end{pmatrix} \right) \\ &= \int \mathbf{E}^{\mathrm{T}} \cdot \mathbf{E}' + \mathbf{H}^{\mathrm{T}} \cdot \mathbf{H}', \end{aligned} \tag{C2}$$

under which the off-diagonal terms in L are still antisymmetric while the diagonal terms are complex-symmetric, assuming *reciprocal materials*: $\varepsilon^{\mathrm{T}} = \varepsilon$ and $\mu^{\mathrm{T}} = \mu$ (usually the case except for magnetooptical and other more exotic materials[82,95,128]). Here, the transpose L^{T} of the operator L means the adjoint of L under the unconjugated inner product $(\phi, L\phi') = (L^{\mathrm{T}}\phi,\phi')$. In order to make L fully symmetric, it suffices to flip the sign of the magnetic components $\mathbf{H} \to -\mathbf{H}$, an operation that can be expressed as a (real, self-adjoint, unitary) sign-flip matrix:

$$\mathcal{S} = \begin{pmatrix} I & \\ & -I \end{pmatrix} = \mathcal{S}^{-1} = \mathcal{S}^{\mathrm{T}} = \mathcal{S}^*. \tag{C3}$$

That is, $L\mathcal{S}$ is complex-symmetric: $(L\mathcal{S})^{\mathrm{T}} = \mathcal{S}L^{\mathrm{T}} = L\mathcal{S}$, or equivalently, $L^{\mathrm{T}} = \mathcal{S}L\mathcal{S} = \mathcal{S}L\mathcal{S}^{-1}$. It follows that

$$(\Gamma\star)^{\mathrm{T}} = (L^{-1})^{\mathrm{T}} = (L^{\mathrm{T}})^{-1} = \mathcal{S}(\Gamma\star)\mathcal{S}. \tag{C4}$$

Alternatively,

$$(\phi, \Gamma \star \phi') = \iint d^3\mathbf{x} d^3\mathbf{y} \phi^{\mathrm{T}}(\mathbf{x})\Gamma(\mathbf{x},\mathbf{y})\phi'(\mathbf{y}), \tag{C5}$$

so by inspection $(\Gamma(\mathbf{x},\mathbf{y})\star)^{\mathrm{T}} = \Gamma(\mathbf{y},\mathbf{x})^{\mathrm{T}}\star$: transposing $\Gamma\star$ corresponds to interchanging sources and fields. Thus we obtain the reciprocity relation

$$\Gamma^{\mathrm{T}}\star = \mathcal{S}(\Gamma\star)\mathcal{S}, \tag{C6}$$

i.e., one can interchange sources and fields if one flips the sign of both magnetic currents and magnetic fields.

We also expect the operators L and $\Gamma\star$ to be negative-semidefinite on physical grounds, since $-\frac{1}{2}\langle\phi,L\phi\rangle = -\frac{1}{2}\langle\phi,\xi\rangle = -\frac{1}{2}\langle\Gamma\star\xi,\xi\rangle$ is exactly the time-average power $-\frac{1}{2}\int \mathbf{E}^*\cdot\mathbf{J}+\mathbf{H}^*\cdot\mathbf{M}$ expended *by* the currents, which must be $\geqslant 0$ in passive materials.[84] Indeed, one can show this directly, since the anti-Hermitian property of the off-diagonal part of L means that

$$\mathrm{sym}L = \omega\begin{pmatrix} -\mathrm{Im}\varepsilon & \\ & -\mathrm{Im}\mu \end{pmatrix}$$

for isotropic materials, but both $\omega\mathrm{Im}\varepsilon$ and $\omega\mathrm{Im}\mu$ are $\geqslant 0$ for passive materials (no gain).[83,84] Thus it follows that L is negative-semidefinite, and so is $L^{-1} = \Gamma\star$.

2. SIE matrices

The SIE matrices $M = W^{-1}$ are formed from a sum $\mathcal{M}$ of Green's function operators $\Gamma^r\star$ in homogeneous regions r, expanded in a (real vector-valued) basis β_n by a Galerkin method, so that $M_{mn} = \langle\beta_m,\mathcal{M}\beta_n\rangle = (\beta_m,\mathcal{M}\beta_n)$. For any Galerkin method, it is easy to show that if $\mathcal{M}$ is self-adjoint or complex-symmetric, then M has the same properties. Similarly, any definiteness of $\mathcal{M}$ carries over to M. From the previous section, since Γ^r is negative-semidefinite in any passive medium, it follows that any sum $\mathcal{M}$ of $\Gamma^r\star$ is also negative-semidefinite, and hence $\mathcal{M}$ is negative-semidefinite (sym$M$ is Hermitian negative-semidefinite).

As above, reciprocity requires some sign flips: $\mathcal{M}^{\mathrm{T}} = S\mathcal{M}S$, so $(M^{\mathrm{T}})_{mn} = M_{nm} = (\beta_n,\mathcal{M}\beta_m) = (\beta_m,\mathcal{M}^{\mathrm{T}}\beta_n) = (\beta_m,S\mathcal{M}S\beta_n) = (S\beta_m,\mathcal{M}S\beta_n)$. Furthermore, suppose that we use separate basis functions β_n^H for magnetic currents and β_n^E for electric currents, as is typically the case in BEM (e.g., for an RWG basis[26,93]), so that $S\beta_n^E = +\beta_n^E$ and $S\beta_n^H = -\beta_n^H$. That is, we write currents as $\xi = \sum_n x_n\beta_n = \sum x_n^E\beta_n^E + x_n^H\beta_n^H$, so that $S\xi = \sum x_n^E\beta_n^E - x_n^H\beta_n^H$ corresponds to a linear transformation S on x that flips the sign of the x_n^H components. It follows that

$$M^{\mathrm{T}} = SMS. \tag{C7}$$

[1] C. Genet, A. Lambrecht, and S. Reynaud, Eur. Phys. J. Special Topics **160**, 183 (2008).

[2] M. Bordag, G. L. Klimchitskaya, U. Mohideen, and V. M. Mostapanenko, *Advances in the Casimir Effect* (Oxford University Press, Oxford, UK, 2009).

[3] A. W. Rodriguez, F. Capasso, and S. G. Johnson, Nat. Phot. **5**, 211 (2011).

[4] S. M. Rytov, V. I. Tatarskii, and Y. A. Kravtsov, *Principles of Statistical Radiophsics II: Correlation Theory of Random Processes* (Springer-Verlag, Berlin, 1989).

[5] D. Polder and M. Van Hove, Phys. Rev. B **4**, 3303 (1971).

[6] J. J. Loomis and H. J. Maris, Phys. Rev. B **50**, 18517 (1994).

[7] J. B. Pendry, J. Phys.: Condens. Matter **11**, 6621 (1999).

[8] A. Kittel, W. Muller-Hirsch, J. Parisi, S.-A. Biehs, D. Reddig, and M. Holthaus, Phys. Rev. Lett. **95**, 224301 (2005).

[9] A. Narayanaswamy, S. Shen, and G. Chen, Phys. Rev. B **78**, 115303 (2008).

[10] L. Hu, A. Narayanaswamy, X. Chen, and G. Chen, Appl. Phys. Lett. **92**, 133106 (2008).

[11] A. Narayanaswamy, S. S, L. Hu, X. Chen, and G. Chen, Appl. Phys. A. **96**, 357 (2009).

[12] E. Rousseau, A. Siria, J. Guillaume, S. Volz, F. Comin, J. Chevrier, and J.-J. Greffet, Nat. Phot. **3**, 514 (2009).

[13] S. Shen, A. Narayanaswamy, and G. Chen, Nano Lett. **9**, 2909 (2009).

[14] D. Y. Wilde, F. Formanek, R. Carminati, B. Gralak, P.-A. Lemoine, K. Joilain, J.-P. Mulet, Y. Chen, and J.-J. Greffet, Nature (London) **444**, 740 (2009).

[15] R. S. Ottens, V. Quetschke, S. Wise, A. A. Alemi, R. Lundock, G. Mueller, D. H. Reitze, D. B. Tanner, and B. F. Whiting, Phys. Rev. Lett. **107**, 014301 (2011).

[16] J.-P. Mulet, K. Joulain, R. Carminati, and J.-J. Greffet, Micro. Thermophys. Eng. **6**, 209 (2002).

[17] K. Joulain, J.-P. Mulet, F. Marquier, R. Carminati, and J.-J. Greffet, Surf. Sci. Rep. **57**, 59 (2005).

[18] G. Chen, *Nanoscale Energy Transport and Conversion: A Parallel Treatment of Electrons, Molecules, Phonons, and Photons*, MIT Pappalardo Series in Mechanical Engineering (Oxford University Press, Madison Avenue, NY, 2005).

[19] V. P. Carey, G. Cheng, C. Grigoropoulos, M. Kaviany, and A. Majumdar, Nanoscale Micro. Thermophys. Eng. **12**, 1 (2006).

[20] C. J. Fu and Z. M. Zhang, Int. J. Heat Mass Transf. **49**, 1703 (2006).

[21] A. I. Volokitin and B. N. J. Persson, Rev. Mod. Phys. **79**, 1291 (2007).

[22] Z. M. Zhang, *Nano/Microscale Heat Transfer* (McGraw-Hill, New York, 2007).

[23] S. Basu, Z. M. Zhang, and C. J. Fu, Int. J. Energy Res. **33**, 1203 (2009).

[24] R. F. Harringston, J. Electromagn. Waves. Appl. **3**, 1 (1989).

[25] W. Hackbush and B. Verlag, *Integral Equations: Theory and Numerical Treatment* (Birkhauser Verlag, Basel, Switzerland, 1995).

[26] S. M. Rao and N. Balakrishnan, Current Science **77**, 1343 (1999).

[27] M. Bonnet, *Boundary Integral Equation Methods for Solids and Fluids* (Wiley, Chichester, England, 1999).

[28] H. Reid, J. White, and S. G. Johnson, arXiv:1203.0075.

[29] A. Narayanaswamy and G. Chen, Phys. Rev. B **77**, 075125 (2008).

[30] G. Bimonte, Phys. Rev. A **80**, 042102 (2009).

[31] R. Messina and M. Antezza, Phys. Rev. A **84**, 042102 (2011).

[32] M. Kruger, T. Emig, and M. Kardar, Phys. Rev. Lett. **106**, 210404 (2011).

[33] C. Otey and S. Fan, Phys. Rev. B **84**, 245431 (2011).

[34] V. A. Golyk, M. Kruger, and M. Kardar, Phys. Rev. E **85**, 046603 (2012).

[35] M. Kruger, G. Bimonte, T. Emig, and M. Kardar, Phys. Rev. B **86**, 115423 (2012).

[36] S. A. Biehs, F. S. S. Rosa, and P. Ben-Abdallah, Appl. Phys. Lett. **98**, 243102 (2011).

[37] R. Guérout, J. Lussange, F. S. S. Rosa, J.-P. Hugonin, D. A. R. Dalvit, J.-J. Greffet, A. Lambrecht, and S. Reynaud, Phys. Rev. B **85**, 180301 (2012).

[38] V. N. Marachevsky, J. Phys. A: Math. Theor. **45**, 374021 (2012).

[39] A. W. Rodriguez, O. Ilic, P. Bermel, I. Celanovic, J. D. Joannopoulos, M. Soljacic, and S. G. Johnson, Phys. Rev. Lett. **107**, 114302 (2011).

[40] A. I. Volokitin and B. N. J. Persson, Phys. Rev. B **63**, 205404 (2001).

[41] A. Narayanaswamy and Y. Zheng, J. Quant. Spectrosc. Radiat. Transfer (2013), doi: 10.1016/j.jqsrt.2013.01.002.

[42] A. W. Rodriguez, M. T. H. Reid, and S. G. Johnson, Phys. Rev. B **86**, 220302(R) (2012).

[43] H. Reid, J. White, and S. G. Johnson, Phys. Rev. A **84**, 010503(R) (2011).

[44] W. Eckhardt, Opt. Commun. **41**, 305 (1981).

[45] W. Eckhardt, Phys. Rev. A **29**, 1991 (1984).

[46] M. Tschikin, S. A. Biehs, F. S. S. Rosa, and P. B. Abdallah, Eur. Phys. J. B **85**, 233 (2012).

[47] E. G. Cravalho, C. L. Tien, and R. P. Caren, J. Heat Transfer **89**, 351 (1967).

[48] C. M. Hargreaves, Phys. Lett. **30**, 491 (1969).

[49] G. A. Domoto, R. F. Boehm, and C. L. Tien, J. Heat Transfer **92**, 412 (1970).

[50] J. L. Pan, H. K. Choy, and C. G. Fonstad, IEEE Trans. Electron Devices **47**, 241 (2000).

[51] M. Laroche, R. Carminati, and J. J. Greffet, J. Appl. Phys. **100**, 063704 (2006).

[52] C. W. Chang, D. Okawa, A. Majumdar, and A. Zettl, Science **314**, 1121 (2006).

[53] C. R. Otey, W. T. Lau, and S. Fan, Phys. Rev. Lett. **104**, 154301 (2010).

[54] S. Basu and M. Francoeur, Appl. Phys. Lett. **98**, 113106 (2011).

[55] H. Iizuka and S. Fan, J. Appl. Phys. **112**, 024304 (2012).

[56] B. J. Lee, Y. B. Chen, and Z. M. Zhang, J. Quant. Spectrosc. Radiat. Transfer **109**, 608 (2008).

[57] W. A. Challener, C. Peng, A. V. Itagi, D. Karns, W. Peng, Y. Peng, X. Yang, X. Zhu, N. J. Gokemeijer, Y. T. Hsia *et al*., Nature (London) **3**, 220 (2009).

[58] A. Kittel, U. F. Wischnath, J. Welker, O. Huth, F. Rüting, and S.-A. Biehs, Appl. Phys. Lett. **93**, 193109 (2008).

[59] S.-A. Biehs, O. Huth, F. Ruting, and M. Holthaus, J. Appl. Phys. **108**, 014312 (2010).

[60] X. J. Wang, S. Basu, and Z. M. Zhang, J. Phys. D: Appl. Phys. **42**, 245403 (2009).

[61] O. Ilic, M. Jablan, J. D. Joannopoulos, I. Celanovic, H. Buljan, and M. Soljacic, Phys. Rev. B **85**, 155422 (2012).

[62] S. A. Biehs, M. Tschikin, and P. B. Ben-Abdallah, Phys. Rev. Lett. **109**, 104301 (2012).

[63] P. J. van Zwol, K. Joulain, P. Ben-Abdallah, and J. Chevrier, Phys. Rev. B **84**, 161413 (2011).

[64] S. A. Biehs, D. Redding, and M. Holthaus, Eur. Phys. J. B **55**, 237 (2007).

[65] M. Francoeur, M. P. Menguc, and D. Vaillon, Appl. Phys. Lett. **93**, 043109 (2008).

[66] C. J. Fu and W. C. Tan, J. Quant. Spectrosc. Radiat. Transfer **110**, 1027 (2009).

[67] S. Basu and M. Francoeur, Appl. Phys. Lett. **98**, 243120 (2011).

[68] P. Ben-Abdallah, K. Joulain, and A. Pryamikov, Appl. Phys. Lett. **96**, 143117 (2010).

[69] A. P. McCauley, M. T. Homer Reid, M. Kruger, and S. G. Johnson, Phys. Rev. B **85**, 165104 (2012).

[70] P.-O. Chapuis, M. Laroche, S. Volz, and J.-J. Greffet, Phys. Rev. B **77**, 125402 (2008).

[71] A. Perez-Madrid, L. C. Lapas, and J. M. Rubi, Phys. Rev. Lett. **103**, 048301 (2009).

[72] G. Domingues, S. Volz, K. Joulain, and J. J. Greffet, Phys. Rev. Lett. **94**, 085901 (2005).

[73] A. Perez-Madrid, J. M. Rubi, and L.C. Lapas, Phys. Rev. B **77**, 155417 (2008).

[74] A. Manjavacas and F. J. Garcias de Abajo, Phys. Rev. B **86**, 075466 (2012).

[75] O. Huth, F. Ruting, S.-A. Biehs, and M. Holthaus, Eur. Phys. J. Appl. Phys. **50**, 10603 (2010).

[76] P. Ben-Abdallah, S.-A. Biehs, and K. Joulain, Phys. Rev. Lett. **107**, 114301 (2011).

[77] B. Bellomo, R. Messina, D. Felbacq, and M. Antezza, Phys. Rev. A **87**, 012101 (2013).

[78] S.-A. Biehs, O. Huth, and F. Rüting, Phys. Rev. B **78**, 085414 (2008).

[79] F. Rüting, S.-A. Biehs, O. Huth, and M. Holthaus, Phys. Rev. B **82**, 115443 (2010).

[80] A. W. Rodriguez, M. T. Homer Reid, J. Varela, J. D. Joannopoulos, F. Capasso, and S. G. Johnson, Phys. Rev. Lett. **110**, 014301 (2013).

[81] S. G. Johnson, in *Casimir Physics*, edited by D. Dalvit, P. Milonni, D. Roberts, and F. d. Rosa, Lecture Notes in Physics Vol. 836 (Springer, Berlin, 2011), Chap. 6, pp. 175–218.

[82] E. M. Lifshitz and L. P. Pitaevskii, *Statistical Physics: Part 2* (Pergamon, Oxford, 1980).

[83] J. D. Jackson, *Classical Electrodynamics*, 3rd ed. (Wiley, New York, 1998).

[84] L. D. Landau, E. M. Lifshitz, and L. P. Pitaevskiĭ, *Electrodynamics of Continuous Media* (Pergamon Press, Oxford, 1960), Vol. 8.

[85] A. E. H. Love, Phi. Trans. Roy. Soc. London **197**, 1 (1901).

[86] J. A. Stratton and L. J. Chu, Phys. Rev. **56**, 99 (1939).

[87] S. Rengarajan and Y. Rahmat-Samii, IEEE Antennas Propag. Mag. **42**, 122 (2000).

[88] D. E. Merewether, R. Fishes, and F. W. Smith, IEEE Trans. Nucl. Sci. **27**, 1829 (1980).

[89] K.-M. Chen, IEEE Trans. Microwave Theory Tech. **37**, 1576 (1989).

[90] K. Umshankar, A. Raflove, and S. Rao, IEEE Trans. Antennas Propag. **34**, 758 (1986).

[91] L. N. Medgyesi-Mitschang, J. M. Putnam, and M. E. Gedera, J. Opt. Soc. Am. A **11**, 1383 (1994).

[92] Typically, the surface-current vector fields are chosen to be either "all-electric" or "all-magnetic", i.e., $\beta^r_{nE} = \binom{\mathbf{b}_n}{0}, \beta^r_{nM} = \binom{0}{\mathbf{b}_n}$, where $\mathbf{b}_n$ is the usual three-component RWG function corresponding to the nth internal edge in a surface mesh. However, in principle, nothing precludes the use of mixed electric-magnetic surface-current basis functions.

[93] S. Rao, D. Wilton, and A. Glisson, IEEE. Trans. Antennas Propag. **30**, 409 (1982).

[94] J. P. Boyd, *Chebychev and Fourier Spectral Methods*, 2nd ed. (Dover, New York, 2001).

[95]A. Serdyukov, I. Semechnko, S. Tretyakov, and A. Sihvola, *Electromagnetics of Bi-anisotropic materials: Theory and applications* (Gordon and Breach Science Publishers, Tokyo, 2001).
[96]L. N. Trefethen and D. Bau, *Numerical Linear Algebra*, 1st ed. (SIAM, Philadelphia, 1997).
[97]G. W. Kattawar and M. Eisner, Appl. Opt. **9**, 2685 (1970).
[98]W. C. Chew, J. M. Jin, E. Michelssen, and J. M. Song, IEEE Trans. Antennas Prop. **45**, 533 (1997).
[99]W. C. Chew, J. Jian-Ming, E. Michielssen, and S. Jiming, *Fast and Efficient Algorithms in Computational Electromagnetics* (Artech, Norwood, MA, 2001).
[100]W. Cai, Y. Yu, and X. C. Yuan, Intl. J. Numer. Meth. Eng. **53**, 31 (2002).
[101]D. J. Taylor, IEEE Trans. Antennas Propag. **51**, 1630 (2003).
[102]M. S. Tong and W. C. Chew, Microwave Opt. Tech. Lett. **49**, 1383 (2006).
[103]R. Barrett, M. Berry, T. F. Chan, J. Demmel, J. Donato, j. Dongarra, V. Eijkhout, R. Pozo, C. Romine, and H. Van der Vorst, *Templates for the Solution of Linear Systems: Building Blocks for Iterative Methods*, 2nd ed. (SIAM, Philadelphia, 1994).
[104]S. J. Rahi, T. Emig, N. Graham, R. L. Jaffe, and M. Kardar, Phys. Rev. D **80**, 085021 (2009).
[105]C. T. Tai, *Dyadic Green's Functions in Electromagnetic Theory* (IEEE Press, Piscataway, NJ, 1993).
[106]P. H. Pathak, IEEE Trans. Antennas Propag. **AP-31**, 837 (1983).
[107]Mathematically, the δ function terms arising in the spectral expansion of the homogeneous DGF arise because the vector-valued basis functions **M** and **N** only span the transverse part of the space and have no components along the longitudinal directions.[105]
[108]M. T. H. Reid (2012), http://homerreid.ath.cx/scuff-em/.
[109]P. Ben-Abdallah, K. Joulain, J. Drevillon, and G. Domingues, J. Appl. Phys. **106**, 044306 (2009).
[110]F. Reif, *Fundamentals of Statistical and Thermal Physics* (McGraw-Hill Series in Fundamentals of Physics, New York, 1965).
[111]H. C. van de Hulst, *Light Scattering by Small Particles* (Dover Publications, New York, 1957).
[112]J. Venermo and A. Sihvola, J. Electrost. **63**, 101 (2005).
[113]A. P. McCauley, Ph.D. thesis, Massachusetts Institute of Technology, 2011.
[114]K. Sasihithlu and A. Narayanaswamy, Phys. Rev. B **83**, 161406(R) (2013).
[115]E. Saidi, B. Samson, L. Aigouy, S. Volz, P. Low, C. Bergaud, and M. Mortier, Nanotechnology **20**, 115703 (2009).
[116]Y. D. Chong and A. D. Stone, Phys. Rev. Lett. **109**, 063902 (2012).
[117]S. Y. Buhmann and S. Scheel, Phys. Rev. Lett. **100**, 253201 (2008).
[118]J. C. Nedelec and F. Starling, SIAM J. Math. Anal. **22**, 1679 (1991).
[119]A. Taflove and S. C. Hagness, *Computational Electrodynamics: The Finite-Difference Time-Domain Method* (Artech, Norwood, MA, 2000).
[120]M. J. Nicholas, Commun. Math. Sci. **6**, 669 (2008).
[121]T. Arens, K. Sandfort, S. Schmitt, and A. Lechleiter, IMA J. Appl. Math. (2011), doi: 10.1093/imamat/hxr057.
[122]A. Barnett and L. Greengard, BIT Num. Math. **51**, 67 (2011).
[123]For simplicity, we assume a differentiable surface ∂V so that its normal **n** is well defined, but the case of surfaces with corners (e.g., cubical domains) follows as a limiting case.
[124]C. Altman and K. Such, *Reciprocity, Spatial Mapping and Time Reversal in Electromagnetics* (Kluwer, Dordrecht, 1991).
[125]A. Karlson and G. Kristensson, J. Electromagn. Waves. Appl. **6**, 537 (1992).
[126]M. Born and E. Wolf, *Principles of Optics: Electromagnetic Theory of Propagation, Interference and Diffraction of Light*, 7th ed. (Cambridge University Press, Cambridge, 1999).
[127]R. J. Potton, Rep. Prog. Phys. **67**, 717 (2004).
[128]R. W. P. King, *Fundamental Electromagnetic Theory* (Dover, New York, 1963).